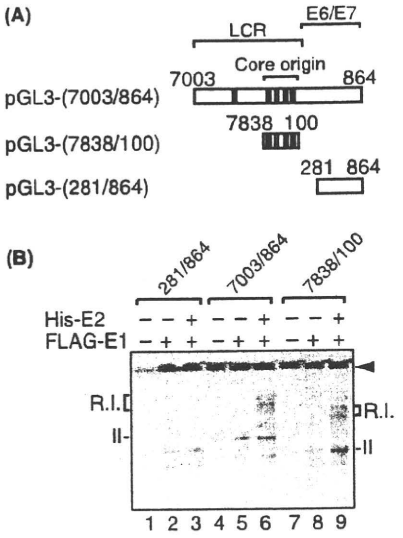


**Figure 6** HPV16 genome regions required for rolling circle replication. (A) A diagram of HPV16 DNA fragments. The fragments were cloned into pGL3 plasmid, and the plasmids were used as replication templates. Numbers above the fragments indicate nucleotide positions in the HPV16 genome. Binding sites for E1 (open box) and E2 (closed box) are indicated. The brackets show the core origin, the long control region and E6/E7 region. (B) Replication assay using cytoplasmic extracts from differentiated W12 cells. pGL3-(281/864) (lanes 1–3), pGL3-(7003/864) (lanes 4–6) or pGL3-(7838/100) (lanes 7–9) was incubated in the extract supplemented with FLAG-E1 and/or His-E2 as indicated. Deproteinized DNA products were subjected to agarose gel electrophoresis, and [$^{32}$P]-labeled replicated DNAs were visualized. The positions of replication intermediates (R.I.) and form II of pGL3-(7003/864) and pGL3-(7838/100) (II) are indicated. The arrowhead indicates rolling circle replication products.

origin plasmid. However, as the extract from undifferentiated W12 cells failed to induce efficient HPV16 DNA replication (Fig. 1F), the dependency of HPV16 rolling circle replication on epithelial differentiation has not been confirmed in our cell-free assays.

As the HPV16 rolling circle replication detected in the epithelial cell extracts shows dependency on the origin, E1 and E2, in the same way as bidirectional replication, the two replication modes are thought to share the same initiation mechanism. Hence, we propose a model in which HPV16 rolling circle replication diverges from bidirectional replication by failure of replication termination (Fig. 7). To start replication from the origin, the E1 hexamer encircles a single-stranded DNA at the origin and moves in a 3′ to 5′ direction thereby inducing an unwinding of a duplex DNA by a strand exclusion mechanism (Castella *et al.* 2006; Enemark & Joshua-Tor 2006). In bidirectional replication, two replication forks, moving from the origin, converge near the point antipodal to the origin. Replication proteins at the forks then dissociate from the DNA to allow for completion of replication. One possible mechanism for the induction of HPV16 rolling circle replication is that E1 fails to dissociate from the DNA on collision of two replication forks and displaces the 5′-end of DNA that has been synthesized by the other replication fork, thus allowing a single-stranded circular DNA to serve as a continuous template for rolling circle replication. The inability of the linear template to induce rolling circle replication (Fig. 4) also supports this model. Furthermore, the mixing experiments using HEK293 and W12 cell extracts (Fig. 5) suggest that inhibitory factor(s) for rolling circle replication are included in the HEK293 cell extract and that these factor(s) may help dissociation of E1 from DNA in the final phase of HPV replication. In contrast to the well-defined initiation phase, little is known about the molecular mechanisms for the termination of HPV replication. Thus, our *in vitro* system that can detect HPV16 rolling circle replication may be useful to identify host factors that are necessary for the termination of HPV replication.

Compared to rolling circle replication systems employed by bacteria and other viruses, the HPV16 rolling circle replication described in this study is unique in that it is enhanced not only by a nicked circular template but also by relaxed one. Although precise mechanisms for this enhancement are not clear, using the less optimal template for replication may increase the probability of termination failure thereby leading to an increase in rolling circle replication. Negative supercoils in a circular DNA topologically favor unwinding of a right-handed DNA duplex and permit efficient progression of replication forks, because negative supercoils neutralize positive supercoils generated by unwinding of a DNA duplex ahead of a replication fork (Postow *et al.* 2001). One can therefore assume that a relaxed or nicked circular DNA without negative superhelical contortion is a less optimal substrate for DNA replication compared to a negatively supercoiled template. In this regard, it is worth noting that circular genomes of SV40 and polyoma virus are isolated as a negatively supercoiled DNA from infected cells (Vinograd *et al.* 1965; Keller 1975; Fanning & Zhao 2009). Because most episomal HPV16 genomes in W12 cells are similarly recovered

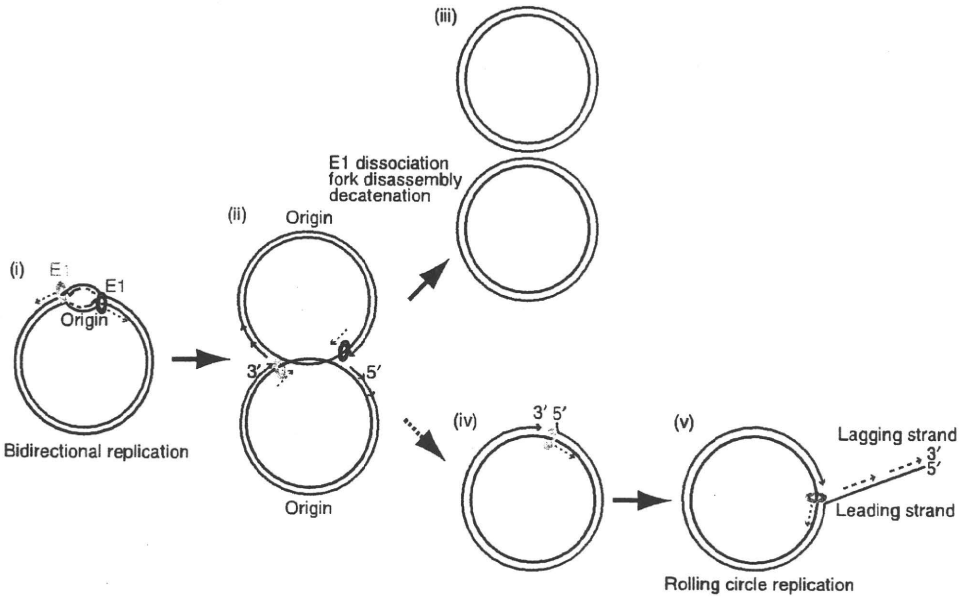


**Figure 7** A model for HPV16 rolling circle replication. (i) E1 binds to the viral origin and starts unwinding the origin DNA to initiate bidirectional replication. (ii) Two replication forks containing E1 converge near the point antipodal to the origin. (iii) Replication proteins and E1 at the forks dissociate from the DNA to allow completion of replication. (iv) When E1 fails to dissociate from the DNA on collision of two replication forks, it accidentally displaces the 5′-end of the DNA strand that has been synthesized by the other replication fork (v) thereby allowing a single-stranded circular DNA to serve as a continuous template for rolling circle replication.

as a supercoiled DNA (Jeon & Lambert 1995; Flores *et al.* 1999), HPV genomes are predicted to be negatively supercoiled in cells and might thus be resistant to rolling circle replication.

Rolling circle replication is widely employed by herpes viruses, such as HSV-1 (Jacob *et al.* 1979; Boehmer & Lehman 1997) and Epstein–Barr virus (Hammerschmidt & Sugden 1988). They have linear DNA genomes of more than 100 kbp, and the linear genome becomes circularized in infected cells to establish latent infection, where the circular genome replicates in a bidirectional mode. In contrast, during the lytic phase of the viral life cycle the replication mode switches to a rolling circle mode, leading to the production of a linear, concatemeric viral genome. Importantly, the genome of these herpes viruses encodes the viral terminase complex that can cleave the concatemeric genome at a specific site to generate unit-length viral genomes for progeny viruses (Homa & Brown 1997). Given that no such virally encoded proteins for cleavage of viral genomes have been identified in HPVs, it seems likely that HPV rolling circle replication is an accidental abortive replication that disrupts the HPV life cycle.

Finally, high-risk HPV DNA is frequently integrated into the chromosome of cervical cancer cells and is occasionally found amplified as head-to-tail tandem repeats (Jeon *et al.* 1995; Pett & Coleman 2007; Lace *et al.* 2009), as typically observed in CaSki cells, which harbor approximately 500 tandem repeats of the HPV16 genome (Callahan *et al.* 1992; Van Tine *et al.* 2004). Although the underlying mechanism behind this type of viral DNA integration is elusive, a plausible explanation is that a linear concatemeric HPV genome is synthesized in cells by a rolling circle mechanism, followed by integration into the host chromosome through cellular pathways for double-strand break repair. Given that nicks in DNA are frequently produced in cells by endogenous reactive oxygen species, nicks arising on the HPV genome may contribute to accidental induction of rolling circle replication of the HPV genome in a cellular environment. Although this hypothesis awaits further experimental investigation, HPV rolling circle replication may have physiological implications for HPV DNA integration into the host chromosome and subsequent progression into cervical cancers.

## Experimental procedures

### Cell culture

W12 cells (clone 20850, W12-E cells) were maintained at subconfluence on mitomycin c-treated J2 3T3 feeder cells in F medium (0.66 mM $Ca^{2+}$) composed of three parts F-12 medium and one part Dulbecco's modified Eagle's medium (DMEM) supplemented with 5% fetal bovine serum (FBS), insulin (5 μg/mL), cholera toxin (8.4 ng/mL), adenine (24 μg/mL), epidermal growth factor (10 ng/mL) and hydrocortisone (0.4 μg/mL) in 5% $CO_2$ at 37 °C. HaCaT and HEK293 cells were grown in DMEM supplemented with 10% FBS in 5% $CO_2$ at 37 °C. To induce differentiation, W12 cells were grown to confluence on J2 3T3 feeder cells in F medium containing 0.66 mM $Ca^{2+}$, then the medium was changed to F medium containing 1.2 mM $Ca^{2+}$ and 10% FBS, followed by further culture for 6 days. HaCaT cells were cultured in DMEM containing 1.8 mM $Ca^{2+}$ and 10% FBS for 6 days. To confirm the differentiation status of cells, expression of cytokeratin 10 or involucrin was examined by Western blotting.

### Preparation of cell extracts

W12, HaCaT and HEK293 cells were scraped in phosphate-buffered saline and washed in ice-cold hypotonic buffer [20 mM HEPES-KOH (pH 7.6), 5 mM KCl, 1.5 mM $MgCl_2$, 1 mM DTT and a protease inhibitor cocktail (Roche Biochemicals)]. The cells were resuspended in an equal volume of hypotonic buffer, incubated on ice for 10 min and homogenized by a Dounce homogenizer with pestle B. The lysate was incubated on ice for 30 min, followed by centrifugation at 10 000 *g* for 10 min. The clarified lysate was used as crude cytoplasmic extracts. The precipitated nuclei were resuspended in an equal volume of hypotonic buffer that had been supplemented with 200 mM NaCl, and incubated on ice for 30 min, followed by centrifugation at 10 000 *g* for 10 min. The resultant supernatant was used as nuclear extracts in Fig. 1F.

### Construction of DNA templates

The modified pUC19, pUC19-B, was constructed by the insertion of a DNA fragment, 5′-GTA CCT CAG CAT G-3′, which contains the recognition sequence for *Bbv*CI, between *Sac*I and *Xba*I sites in pUC19. The template plasmid, pUC19-B-HPV16, was constructed by insertion of the *Pst*I fragment of the HPV16 genome (nucleotide positions 7003 to 880) into the *Pst*I site in pUC19-B. To be used as replication templates, negatively supercoiled pUC19-B-HPV16 and pUC19-B were purified by CsCl-gradient ultracentrifugation. To generate a nicked template, the plasmids were treated with nicking enzymes, Nb.*Bbv*CI or Nt.*Bbv*CI (New England Biolabs). To obtain a linear template, pUC19-B-HPV16 was cleaved with *Hin*dIII, and to obtain a relaxed template, pUC19-B-HPV16 was treated with topoisomerase I (Invitrogen). After the reaction, these enzymes were heat-inactivated. The plasmids containing the HPV16 DNA fragments, pGL3-(7003/864) (previously designated as pGL3-$P_{670}$), pGL3-(7838/100) and pGL3-(281/864) were described previously (Kukimoto *et al.* 2008).

### Preparation of recombinant E1 and E2 proteins

N-terminally FLAG-tagged E1 (FLAG-E1) was purified from Sf9 cells that had been infected with a recombinant baculovirus expressing FLAG-E1. To construct the baculovirus transfer plasmid for the expression of FLAG-E1, the full-length cDNA of HPV16 E1 was amplified by PCR with the template pCMV-$E1_{16}$ (Del Vecchio *et al.* 1992) using primers, 5′-TCC GCG GCC GCT GAT CCT GCT GGC ACC AAT GGG GAA GAG GGT ACG-3′ and 5′-CGT GAG CTC TCA TAA TGT GTT AGT ATT TTG TCC TGA-3′ (*Eag*I and *Kpn*I sites are underlined) and cloned between *Eag*I and *Kpn*I sites of the baculovirus transfer plasmid pAcSG2 (BD Biosciences). The cDNA sequence of a single FLAG-tag was then introduced into the N-terminus of the E1 cDNA. The recombinant baculovirus expressing FLAG-E1 was obtained with the transfer plasmid and the BaculoGold kit (BD Biosciences). Sf9 cells that had been infected with the FLAG-E1-expressing baculovirus were suspended in lysis buffer consisting of 20 mM Tris–HCl (pH 8.0), 500 mM NaCl, 4 mM $MgCl_2$, 0.4 mM EDTA, 2 mM DTT and 20% glycerol, supplemented with a protease inhibitor cocktail (Roche Applied Science) and then disrupted with a Dounce homogenizer. After removal of insoluble material by centrifugation, the clear supernatant was mixed with anti-FLAG M2-conjugated agarose (Sigma, St. Louis, MO, USA) for 4 h at 4 °C. The resin was washed four times with wash buffer consisting of 20 mM Tris–HCl (pH 8.0), 150 mM NaCl, 2 mM $MgCl_2$, 1 mM DTT, 0.2 mM EDTA, 15% glycerol, 0.01% NP-40 and a protease inhibitor cocktail. FLAG-E1 was then eluted with wash buffer containing 0.2 mg/mL FLAG peptide (Sigma). Protein concentration was estimated by SDS-PAGE and staining with GelCode (Pierce).

N-terminally $His_6$-tagged E2 (His-E2) was purified from *E. coli* BL21(DE3) pLysS that had been transformed with an expression plasmid for His-E2. To construct the expression plasmid for His-E2, the full-length cDNA of HPV16 E2 was amplified by PCR with the template pCMV-$E2_{16}$ (Del Vecchio *et al.* 1992) using primers, 5′-GAC GAC GAC AAG ATG GAG ACT CTT TGC CAA CGT T-3′ and 5′-GAG GAG AAG CCC GGT CAT ATA GAC ATA AAT CCA GTA-3′ and cloned into pET-30 (Novagen, Madison, WI, USA) using the Ek/LIC cloning kit (Novagen). Bacterial cells that had been transformed with the expression plasmid were lysed in BugBuster HT Protein Extraction Reagent (Takara Bio Inc.) supplemented with a protease inhibitor cocktail and then incubated for 20 min at room temperature. The lysate was centrifuged at 20 000 *g* for 20 min at 4 °C. Four volumes of buffer A [20 mM sodium phosphate (pH 7.4) and 500 mM NaCl] containing 20 mM imidazole was added to the

supernatant and passed through a 0.44-μm filter. The filtered supernatant was loaded onto a 5 mL HiTrap HP column (GE Healthcare), and bound proteins were eluted on a linear gradient of imidazole from 20 to 500 mM in buffer A. The fractions containing His-E2 were dialyzed against buffer B [20 mM sodium phosphate (pH 7.4), 300 mM NaCl, and 10% glycerol]. Protein concentration was determined by the Bradford assay (Bio-Rad). The purified FLAG-E1 and His-E2 were frozen in liquid nitrogen and stored at −80 °C until use.

### Cell-free replication assay

An *in vitro* HPV16 replication assay was carried out based on the cell-free HPV11 replication assay established by Kuo *et al.* (1994). Briefly, cell extracts (25 μg of W12 or HaCaT extract, or 50 μg of HEK293 extract) were pre-incubated in a 25 μL of replication buffer [30 mM HEPES-KOH (pH 7.6), 0.5 mM DTT, 200 μM each UTP, GTP, CTP and 4 mM ATP, 100 μM each dATP, dGTP, dTTP and 25 μM dCTP, 40 mM phosphocreatine and 10 μg/mL creatine phosphokinase] at 37 °C for 30 min. The replication reaction was initiated by adding 100 ng of FLAG-E1, 1 ng of His-E2, 40 ng of a plasmid template and 37 Bq of [$\alpha$-$^{32}$P] dCTP (111 TBq/mmol) to the reaction mixture, then the mixture was incubated at 37 °C for 2 h. The reaction was terminated by the addition of a stop buffer [20 mM Tris–HCl (pH 7.5), 6 mM EDTA, 0.1% SDS, and 200 μg/mL proteinase K], followed by incubation at 37 °C for 30 min. The reaction mixture was then extracted with phenol–chloroform–isoamyl alcohol (25:24:1), and the DNA in the mixture was precipitated with Pellet Paint Co-Precipitant (Novagen). DNA samples were run on 0.6% agarose gels in 1× Tris–acetate–EDTA buffer. The gels were dried and analyzed by a BAS2500 image analyzer (Fujifilm, Tokyo, Japan). In Fig. 2C, after 0.6% agarose gel electrophoresis, a gel piece containing a high-molecular-weight DNA was excised and incubated at 37 °C for 30 min in buffer containing *Hin*dIII. The gel was embedded in another 1% agarose gel, followed by electrophoresis in 1× Tris–acetate–EDTA buffer.

## Acknowledgements

We thank Drs Paul Lambert and Tomomi Nakahara for the W12 cell line and Dr Peter Howley for the E1 and E2 expression plasmids. This work was supported by a Grant-in-Aid for Young Scientists (Start-up) (20890289) from Japan Society for the Promotion of Science (to R. K.).

## References

Better, M. & Freifelder, D. (1983) Studies on the replication of Escherichia coli phage lambda DNA. I. The kinetics of DNA replication and requirements for the generation of rolling circles. *Virology* **126**, 168–182.

Boehmer, P.E. & Lehman, I.R. (1997) Herpes simplex virus DNA replication. *Annu. Rev. Biochem.* **66**, 347–384.

Callahan, D.E., Karim, A., Zheng, G., Tso, P.O. & Lesko, S.A. (1992) Quantitation and mapping of integrated human papillomavirus on human metaphase chromosomes using a fluorescence microscope imaging system. *Cytometry* **13**, 453–461.

Castella, S., Burgin, D. & Sanders, C.M. (2006) Role of ATP hydrolysis in the DNA translocase activity of the bovine papillomavirus (BPV-1) E1 helicase. *Nucleic Acids Res.* **34**, 3731–3741.

Del Vecchio, A.M., Romanczuk, H., Howley, P.M. & Baker, C.C. (1992) Transient replication of human papillomavirus DNAs. *J. Virol.* **66**, 5949–5958.

Enemark, E.J. & Joshua-Tor, L. (2006) Mechanism of DNA translocation in a replicative hexameric helicase. *Nature* **442**, 270–275.

Fanning, E. & Zhao, K. (2009) SV40 DNA replication: from the A gene to a nanomachine. *Virology* **384**, 352–359.

Faurez, F., Dory, D., Grasland, B. & Jestin, A. (2009) Replication of porcine circoviruses. *Virol. J.* **6**, 60.

Flores, E.R., Allen-Hoffmann, B.L., Lee, D., Sattler, C.A. & Lambert, P.F. (1999) Establishment of the human papillomavirus type 16 (HPV-16) life cycle in an immortalized human foreskin keratinocyte cell line. *Virology* **262**, 344–354.

Flores, E.R. & Lambert, P.F. (1997) Evidence for a switch in the mode of human papillomavirus type 16 DNA replication during the viral life cycle. *J. Virol.* **71**, 7167–7179.

Hammerschmidt, W. & Sugden, B. (1988) Identification and characterization of oriLyt, a lytic origin of DNA replication of Epstein–Barr virus. *Cell* **55**, 427–433.

zur Hausen, H. (1996) Papillomavirus infections – a major cause of human cancers. *Biochim. Biophys. Acta* **1288**, F55–F78.

Homa, F.L. & Brown, J.C. (1997) Capsid assembly and DNA packaging in herpes simplex virus. *Rev. Med. Virol.* **7**, 107–122.

Hubert, W.G., Kanaya, T. & Laimins, L.A. (1999) DNA replication of human papillomavirus type 31 is modulated by elements of the upstream regulatory region that lie 5′ of the minimal origin. *J. Virol.* **73**, 1835–1845.

Jacob, R.J., Morse, L.S. & Roizman, B. (1979) Anatomy of herpes simplex virus DNA. XII. Accumulation of head-to-tail concatemers in nuclei of infected cells and their role in the generation of the four isomeric arrangements of viral DNA. *J. Virol.* **29**, 448–457.

Jeon, S., Allen-Hoffmann, B.L. & Lambert, P.F. (1995) Integration of human papillomavirus type 16 into the human genome correlates with a selective growth advantage of cells. *J. Virol.* **69**, 2989–2997.

Jeon, S. & Lambert, P.F. (1995) Integration of human papillomavirus type 16 DNA into the human genome leads to increased stability of E6 and E7 mRNAs: implications for cervical carcinogenesis. *Proc. Natl Acad. Sci. USA* **92**, 1654–1658.

Kadaja, M., Silla, T., Ustav, E. & Ustav, M. (2009) Papillomavirus DNA replication – from initiation to genomic instability. *Virology* **384**, 360–368.

Kasukawa, H., Howley, P.M. & Benson, J.D. (1998) A fifteen-amino-acid peptide inhibits human papillomavirus E1-E2 interaction and human papillomavirus DNA replication *in vitro*. *J. Virol.* **72**, 8166–8173.

Keller, W. (1975) Determination of the number of superhelical turns in simian virus 40 DNA by gel electrophoresis. *Proc. Natl Acad. Sci. USA* **72**, 4876–4880.

Kukimoto, I., Mori, S., Sato, H., Takeuchi, T. & Kanda, T. (2008) Transcription factor human Skn-1a enhances replication of human papillomavirus DNA through the direct binding to two sites near the viral replication origin. *FEBS J.* **275**, 3123–3135.

Kuo, S.R., Liu, J.S., Broker, T.R. & Chow, L.T. (1994) Cell-free replication of the human papillomavirus DNA with homologous viral E1 and E2 proteins and human cell extracts. *J. Biol. Chem.* **269**, 24058–24065.

Lace, M.J., Isacson, C., Anson, J.R., Lorincz, A.T., Wilczynski, S.P., Haugen, T.H. & Turek, L.P. (2009) Upstream regulatory region alterations found in human papillomavirus type 16 (HPV-16) isolates from cervical carcinomas increase transcription, ori function, and HPV immortalization capacity in culture. *J. Virol.* **83**, 7457–7466.

Lin, B.Y., Ma, T., Liu, J.S., Kuo, S.R., Jin, G., Broker, T.R., Harper, J.W. & Chow, L.T. (2000) HeLa cells are phenotypically limiting in cyclin E/CDK2 for efficient human papillomavirus DNA replication. *J. Biol. Chem.* **275**, 6167–6174.

Longworth, M.S. & Laimins, L.A. (2004) Pathogenesis of human papillomaviruses in differentiating epithelia. *Microbiol. Mol. Biol. Rev.* **68**, 362–372.

Melendy, T., Sedman, J. & Stenlund, A. (1995) Cellular factors required for papillomavirus DNA replication. *J. Virol.* **69**, 7857–7867.

Noirot, P., Bargonetti, J. & Novick, R.P. (1990) Initiation of rolling-circle replication in pT181 plasmid: initiator protein enhances cruciform extrusion at the origin. *Proc. Natl Acad. Sci. USA* **87**, 8560–8564.

Park, P., Copeland, W., Yang, L., Wang, T., Botchan, M.R. & Mohr, I.J. (1994) The cellular DNA polymerase alpha-primase is required for papillomavirus DNA replication and associates with the viral E1 helicase. *Proc. Natl Acad. Sci. USA* **91**, 8700–8704.

Parkin, D.M., Almonte, M., Bruni, L., Clifford, G., Curado, M.P. & Pineros, M. (2008) Burden and trends of type-specific human papillomavirus infections and related diseases in the latin america and Caribbean region. *Vaccine* **26** (Suppl. 11), L1–L15.

Pett, M. & Coleman, N. (2007) Integration of high-risk human papillomavirus: a key event in cervical carcinogenesis? *J. Pathol.* **212**, 356–367.

Postow, L., Crisona, N.J., Peter, B.J., Hardy, C.D. & Cozzarelli, N.R. (2001) Topological challenges to DNA replication: conformations at the fork. *Proc. Natl Acad. Sci. USA* **98**, 8219–8226.

Skaliter, R., Makhov, A.M., Griffith, J.D. & Lehman, I.R. (1996) Rolling circle DNA replication by extracts of herpes simplex virus type 1-infected human cells. *J. Virol.* **70**, 1132–1136.

Stanley, M.A., Browne, H.M., Appleby, M. & Minson, A.C. (1989) Properties of a non-tumorigenic human cervical keratinocyte cell line. *Int. J. Cancer* **43**, 672–676.

Stenlund, A. (2003) Initiation of DNA replication: lessons from viral initiator proteins. *Nat. Rev. Mol. Cell Biol.* **4**, 777–785.

Van Tine, B.A., Kappes, J.C., Banerjee, N.S., Knops, J., Lai, L., Steenbergen, R.D., Meijer, C.L., Snijders, P.J., Chatis, P., Broker, T.R., Moen, P.T. Jr & Chow, L.T. (2004) Clonal selection for transcriptionally active viral oncogenes during progression to cancer. *J. Virol.* **78**, 11172–11186.

Vinograd, J., Lebowitz, J., Radloff, R., Watson, R. & Laipis, P. (1965) The twisted circular form of polyoma viral DNA. *Proc. Natl Acad. Sci. USA* **53**, 1104–1111.

Walther, A.P., Bjerke, M.P. & Wold, M.S. (1999) A novel assay for examining the molecular reactions at the eukaryotic replication fork: activities of replication protein A required during elongation. *Nucleic Acids Res.* **27**, 656–664.

*Received:* 6 August 2010
*Accepted:* 22 September 2010

Jpn. J. Infect. Dis., 63, 25-30, 2010

**Original Article**

# Induction of Indistinguishable Gene Expression Patterns in Rats by Vero Cell-Derived and Mouse Brain-Derived Japanese Encephalitis Vaccines

Haruka Momose†, Jun-ichi Imai[1]†, Isao Hamaguchi†, Mika Kawamura[1,2], Takuo Mizukami, Seishiro Naito, Atsuko Masumi, Jun-ichi Maeyama, Kazuya Takizawa, Madoka Kuramitsu, Nobuo Nomura[3], Shinya Watanabe[1], and Kazunari Yamaguchi*

*Department of Safety Research on Blood and Biological Products, National Institute of Infectious Diseases, Tokyo 208-0011; [1]Department of Clinical Informatics, Tokyo Medical and Dental University, Tokyo 133-8519; [2]Medicrome, Inc., Tokyo 151-0051; and [3]Biological Information Research Center, National Institute of Advanced Industrial Science and Technology, Tokyo 135-0064, Japan*

(Received July 8, 2009. Accepted November 12, 2009)

**SUMMARY**: Transcriptomics is an objective index that reflects the overall condition of cells or tissues, and transcriptome technology, such as DNA microarray analysis, is now being introduced for the quality control of medical products. In this study, we applied DNA microarray analysis to evaluate the character of Japanese encephalitis (JE) vaccines. When administered into rat peritoneum, Vero cell-derived and mouse brain-derived JE vaccines induced similar gene expression patterns in liver and brain. Body weights and blood biochemical findings were also similar after administration of the two vaccines. Our results suggest that the two JE vaccines are likely to have equivalent characteristics with regard to reactivity in rats.

## INTRODUCTION

Japanese encephalitis (JE) is a seasonal and sporadic viral encephalitis in East Asia, caused by infection with the JE virus. The JE virus exists in a zoonotic cycle between mosquitoes and swine and/or water birds. Infectious mosquitoes transmit JE to humans, a dead-end host (1). The great majority of infections are not apparent; the incidence of JE is considered to be 1 case per 250 to 500 infections (2). Even if the disease becomes manifest, recovery from mild illness occurs in most cases. Severe infection can cause febrile headache syndrome, aseptic meningitis, or encephalitis after an incubation period of about 6 to 16 days (1). Once JE has developed, the fatality rate is relatively high, from 5 to 40%, depending on the outbreak. Permanent neurological or psychiatric sequelae are left in 45–70% of survivors (1–3). No specific treatments for JE are available; therefore, preventing virus infection with vaccination is the most effective form of defense.

The approved and widely used JE vaccine is manufactured from inactivated JE virus that has been propagated in mouse brain. This mouse brain-derived (MBD) vaccine is currently manufactured and used in Japan, Korea, Taiwan, Thailand, Vietnam, and India, and is licensed in the United States, Canada, Israel, Australia, and several other Asian countries. Vaccination has succeeded in the near elimination of JE in several countries.

The MBD JE vaccine is a very pure form; impurities are removed during the manufacturing process, especially brain-derived matter (3). Thus the vaccine has been considered safe. However, adverse reactions, such as local reactions and mild systemic events, may occur in 10–30% of vaccinated subjects (3). Acute disseminated encephalomyelitis (ADEM) coinciding with the administration of MBD vaccines has been reported at frequencies of 1 to 2 out of 100,000 doses (2,3). In the wake of a severe case of ADEM, the recommendation for a program of routine childhood immunization against JE was suspended in Japan in 2005 (2,4). It is of great concern that non-immunized children are not given the JE vaccine in JE-infected areas of Japan.

To replace the current MBD vaccine, Vero cell-derived (VCD) vaccines have been developed (5–10). The cessation of using mouse brain for virus propagation is expected to reduce the incidence of severe adverse reactions, including ADEM, because myelin basic protein, which is abundant in the central nervous system, is a possible substrate that provokes ADEM (11). Further, a cell culture-based technique is advantageous for large-scale production of JE vaccine. The demand for JE vaccine is growing, because the distribution of the JE virus has expanded throughout Asia and towards the northern edge of Australia over the last decade (12,13), and these newly JE virus-infected countries will require JE vaccine.

Apart from these concerns about the JE vaccine, moving towards cell culture-based vaccines is a global trend in the field of virus vaccine development (14). Primary hamster kidney cells were the first cells to be accepted for the production of JE vaccine, and continue to be used in China and some other countries (3,15). Recently, vaccine production using primary cell culture systems has been replaced by production using continuous cell lines (CCLs), including the Vero cell line (14). The Vero cell line is the most widely accepted CCL by regulatory authorities and has been used for over 30 years for the production of polio and rabies virus vaccines (16,17). In addition, VCD vaccines for rotavirus, smallpox

*Corresponding author: Mailing address: Department of Safety Research on Blood and Biological Products, National Institute of Infectious Diseases, 4-7-1 Gakuen, Musashimurayama, Tokyo 208-0011, Japan. Tel: +81-42-561-0771, Fax: +81-42-565-3315, E-mail: kyama@nih.go.jp

†These authors contributed equally to the paper.

virus, and influenza virus have been developed (14,18). In the case of JE vaccines, one of the developed VCD vaccines has received recent approval in the United States and Europe. Another was licensed in Japan in February 2009.

A newly licensed VCD JE vaccine must be at least equivalent to the current high-quality MBD vaccine in effectiveness. In this study, we applied conventional animal tests to demonstrate the equivalence of the MBD JE vaccine and the VCD JE vaccine. Further, based on our previous studies demonstrating that DNA microarray analysis was able to assay the features of a vaccine with high sensitivity, comprehensive gene expression analysis was performed to characterize the physiological reactivity of both JE vaccines.

## MATERIALS AND METHODS

**Animals**: Eight-week-old male Wistar rats, weighing 160–200 g, were obtained from SLC (Tokyo, Japan). Animals were housed in rooms maintained at 23 ± 1°C, with 50 ± 10% relative humidity and 12-h light/dark cycles, for at least 1 week prior to the test challenge. All procedures used in this study complied with institutional policies of the Animal Care and Use Committee of the National Institute of Infectious Diseases.

**Vaccines**: The approved JE vaccine (MBD) is an inactivated, highly purified JE virus (Beijin-1 strain), propagated in mouse brain. The improved inactivated vaccine (VCD) is manufactured from the same strain in Vero cells. Both vaccines were generous gifts from Biken, The Research Foundation for Microbial Diseases of Osaka University, Japan. We administered 5 ml of MBD or VCD into rat peritoneum. Physiological saline (SA) was used as a control.

**Weight check**: The rat decreasing body weight test was performed according to the Minimum Requirements for Biological Products in Japan (19). After we injected 5 ml of samples into the peritoneum, animals were weighed daily. Five rats in each group were used.

**Hematological test**: Rats were treated with SA, MBD, or VCD, and blood samples were collected on days 1, 2, 3, and 4 after administration. Blood was immediately mixed with EDTA, and the number of erythrocytes, hematocrit level, hemoglobin value, number of leukocytes, and number of platelets (PLT) were determined using an automatic hematocytometer, the Celltac MEK-5254 (Nihon Kohden, Tokyo, Japan). Five rats in each group were used.

**Serum test**: Blood samples for the serum test were collected separately from the same rats used for the hematological test. After centrifugation at 3,000 rpm for 15 min, 10-fold diluted supernatants were used for subsequent tests. We measured the activity of glutamate oxaloacetate transaminase/aspartate aminotransferase (GOT/AST), glutamate pyruvate transaminase/alanine aminotransferase (GPT/ALT), alkaline phosphatase (ALP), amylase (AMYL), and creatine phosphokinase (CPK), and the quantity of blood urea nitrogen (BUN), creatinine (CRE), total cholesterol (TCHO), triglyceride (TG), glucose (GLU), and C-reactive protein (CRP) using a DRICHEM-3030 according to the manufacturer's instructions (Fujifilm, Japan). Five rats in each group were used.

**RNA preparation**: Rats were sacrificed to obtain the whole brain and the lateral left lobe of the liver. Tissues were immediately frozen in liquid nitrogen for storage. Thawed tissue was homogenized and mixed with Isogen reagent (NIPPON GENE, Tokyo, Japan). Total RNA was prepared from the lysate in accordance with the manufacturer's instructions. Poly(A)$^+$ RNA was prepared from total RNA with a Poly(A) Purist Kit (Ambion, Austin, Tex., USA) according to the manufacturer's instructions.

**Microarray preparation and expression profile acquisition**: For microarray analysis, rats were treated with SA, MBD, or VCD (3 rats per treatment), and 2 tissue samples from each animal, brain and liver, were analyzed on days 1–4 post-treatment. A set of synthetic polynucleotides (80-mers) representing 11,468 rat transcripts and including most of the RefSeq genes deposited in the NCBI database (MicroDiagnostic, Tokyo, Japan) was arrayed on aminosilane-coated glass slides (Type I; Matsunami, Kishiwada, Japan) with a custom-made arrayer (20,21). Poly(A)$^+$ RNA (1.5 $\mu$g) of each sample was labeled using SuperScript II (Invitrogen, Carlsbad, Calif., USA) with Cyanine 5-dUTP. A common reference RNA (MicroDiagnostic) was labeled with Cyanine 3-dUTP (PerkinElmer, Boston, Mass., USA). Labeling, hybridization, and washes of microarrays were performed with a Labeling & Hybridization Kit (MicroDiagnostic) according to the manufacturer's instructions. The common reference RNA was purchased as a single batch and was labeled with Cyanine-3 for a single microarray side by side with each sample labeled with Cyanine-5. Hybridization signals were measured using a GenePix 4000A scanner (Axon Instruments, Union City, Calif., USA) and then processed into primary expression ratios ([Cyanine 5-intensity obtained from each sample]/[Cyanine 3-intensity obtained from common reference RNA], which are indicated as 'median of ratios' in GenePix Pro 3.0 software [Axon Instruments]). The GenePix Pro 3.0 software performed normalization for the median of ratios (primary expression ratios) by multiplying normalization factors calculated for each feature on a microarray.

**Data analysis**: Data processing and hierarchical cluster analysis were performed using Excel (Microsoft, Redmond, Wash., USA) and an MDI gene expression analysis software package (MicroDiagnostic). The primary expression ratios were converted into $\log_2$ values ($\log_2$ Cyanine-5 intensity/Cyanine-3 intensity) (designated log ratios) and compiled into a matrix (designated primary data matrix). To predict the most obvious differences obtained from cluster analysis of the primary data matrix, we extracted genes with $\log_2$ ratios over 1 or under −1 in at least 1 sample from the primary data matrix and subjected them to two-dimensional hierarchical cluster analysis for samples and genes.

To identify genes demonstrating significant changes in expression, we extracted genes by $t$ test between SA- and MBD-, SA- and VCD-, or MBD- and VCD-treated samples ($P < 0.01$).

## RESULTS

**Vaccine-treated animals showed no weight loss**: Vaccines for public use are all made according to Good Manufacturing Practice (GMP), and many tests must be done before releasing vaccines to assure their quality. Conventional animal tests including the decreasing body weight test are applied for the quality control of vaccines (19). To explore the effects of the JE vaccines in a conventional method, we first applied the decreasing body weight test to the MBD and VCD JE vaccines, as described in Minimum Requirements for Biological Products in Japan (19). For this test, 5 ml of the vaccine was injected into the rat peritoneum, and the weight of the treated rats was measured daily for 4 days. As shown in Fig. 1, VCD-treated rats (filled circles) did not show

any weight loss, and gained weight in a similar manner to that of the SA- and MBD-treated groups (open and gray squares, respectively). Further, no abnormalities were observed in the condition or behavior of the rats during the testing period. Severe toxicity of MBD and VCD was not detected from this test.

**Hematological tests revealed no significant changes in vaccinated rats**: To investigate the influence of JE vaccines on hematological parameters, we treated rats with SA, MBD, or VCD (5 rats per treatment) and collected blood samples on days 1, 2, 3, and 4 after administration. We counted erythrocytes, leukocytes, and PLT and measured hematocrit levels and hemoglobin values. At any time point, all characteristics examined were within normal ranges and showed no significant differences among SA-, MBD-, and VCD-treated groups (Fig. 2). These results indicated that neither MBD nor VCD exhibited hematotoxicity to the treated rats.

**Normal levels were observed in serum tests in vaccine-treated rats**: To evaluate the reactivity of JE vaccines on biological functions, we performed serum tests on vaccine-administered rats. On days 1, 2, 3, and 4 after administration of SA, MBD, or VCD, we collected blood from the same rats used for hematological tests, and isolated serum. Each serum sample was tested for liver function, renal function, muscle dysfunction, and metabolic abnormalities. No significant increase was observed in GOT/AST, GPT/ALT, ALP, or AMYL in any samples tested, indicating that no liver damage had occurred (Fig. 3 top panels). CRP values were all below detection limits (data not shown). Tests of renal (BUN and CRE) and muscle (CPK) function and of metabolism (TCHO, TG, and GLU) showed no differences among the vaccine-treated groups (Fig. 3 middle and bottom panels). These results suggested that SA, MBD, and VCD had similar biological reactivity in rats.

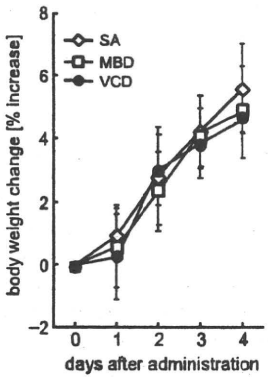


Fig. 1. Body weight analysis of the JE vaccine treated animals. The effects of mouse brain-derived (MBD) JE vaccine, Vero cell-derived (VCD) JE vaccine, and saline (SA) treatment were measured using decreasing body weight toxicity tests. All rats were weighed at days 0, 1, 2, 3, and 4. Changes in rat body weight were assessed as the percentage increase or decrease, and are indicated by the mean change ± S.D.

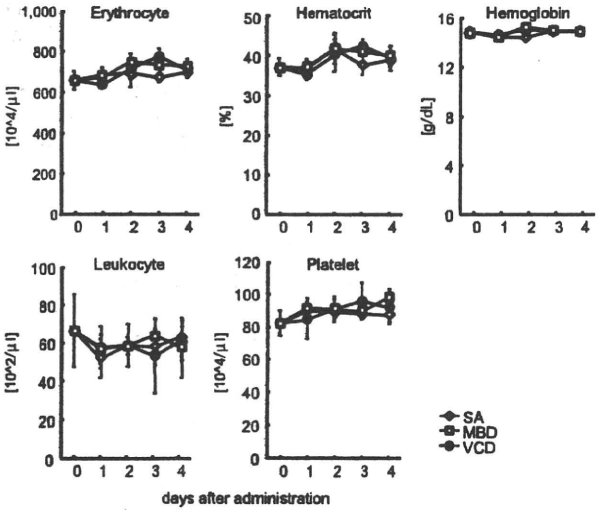


Fig. 2. Hematological tests for vaccinated rats. Blood obtained from individual rats was subjected to hematological tests. The tests were performed for 4 consecutive days after SA (open square), MBD (gray square), and VCD (filled circle) administration. Values are expressed as mean ± S.D.

**Microarray analysis of tissues from vaccine-treated rats**: Although the animal tests described above have long been accepted for the quality control of biological reagents (22–24), the progress of molecular biotechnology presents the possibility to improve or renew the traditional tests. Among recent technologies, the high-throughput 'omics'-based technologies have led the way to clarify immune responses to pathogens and responses of metabolic pathways, as well as to develop new vaccine candidates (25–27). Now, several efforts have been made to analyze the side effects of pharmaceuticals using one of the 'omics' technologies, transcriptomics (28,29). In this context, we performed DNA microarray analysis of the vaccinated rat tissues, liver and brain, and tried to determine the effects of MBD and VCD by analyzing gene expression patterns. The liver is thought to be one of the most appropriate organs to analyze biological alterations due to vaccination, because it is the major organ of metabolism. The brain was taken as another target tissue because a neurological effect can be one of the side effects of JE vaccination.

For the analysis, SA-, MBD-, and VCD-treated rats (3 rats per group) were sacrificed to obtain the liver and brain on days 1, 2, 3, and 4 post-administration. Thirty-six samples from each tissue type were obtained. Poly(A)$^+$ RNA purified from the samples and a rat common reference RNA were labeled with Cyanine-5 and Cyanine-3, respectively, and hybridized to microarrays representing 11,468 transcripts. Hybridization signals were processed into expression ratios as $\log_2$ values (designated log ratios) and compiled into a matrix designated as the primary data matrix (see Materials and Methods).

To predict the most obvious differences obtained from the cluster analysis, we extracted genes with log ratios over 1 or under −1 in at least 1 sample in each group. Eventually, 2,386 genes for liver and 4,075 genes for brain were extracted and subjected to two-dimensional hierarchical cluster analysis for samples and genes (Fig. 4A). With hierarchical cluster analysis, genes were grouped according to expression patterns; thus samples having a similar gene expression pattern were clustered together, and samples having a distinct gene expression pattern formed a separate cluster (Fig. 4A) (30–32). If all test samples showed similar gene expression patterns, no clear clusters were formed. Thus, whether distinct clusters were formed was the criterion for the assessment of whether treatment with the 2 vaccines induced different gene expression patterns. Each column represents a sample. Each row represents a gene, and gene expression values are typically illustrated by a colored rectangle, red for up-regulation, blue for down-regulation, and yellow for no change. As shown, no

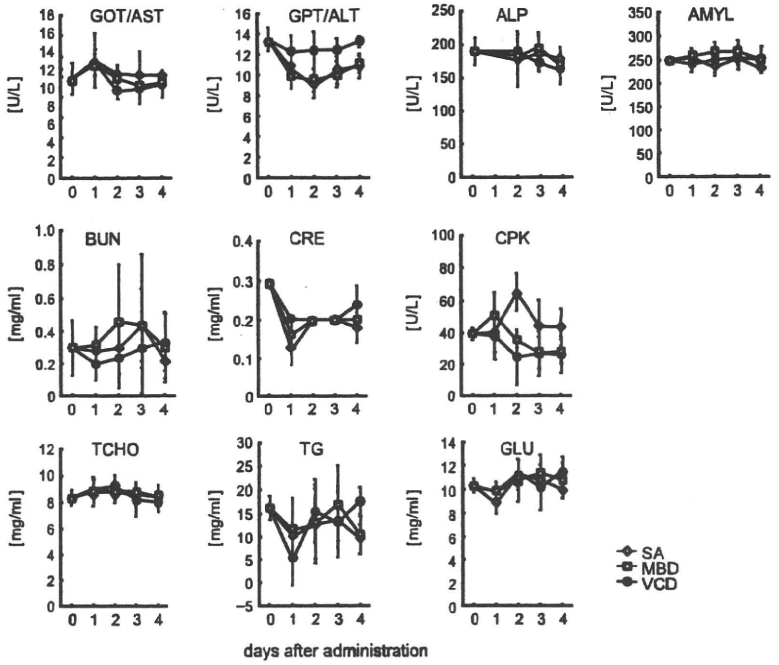


Fig. 3. Serum tests for vaccinated rats. Serum was separated from blood obtained from individual rats, and subjected to serum tests. The tests were performed for 4 consecutive days after SA (open square), MBD (gray square), and VCD (filled circle) administration. Values are expressed as mean ± S.D.

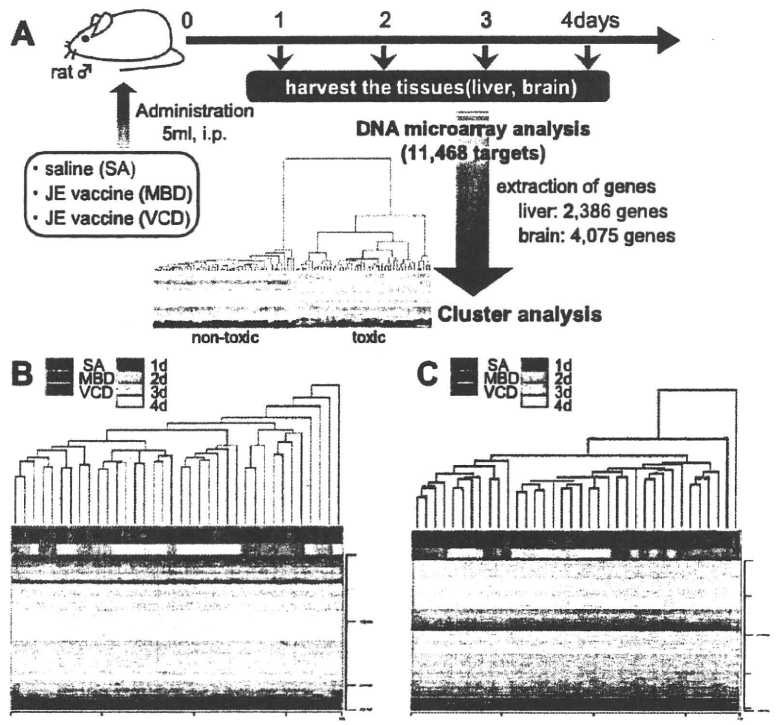


Fig. 4. Gene expression profiling and cluster analysis of vaccine-treated rat tissues. The procedure for gene expression analysis is outlined in A. For the cluster analysis, 2,386 genes for liver (B) and 4,075 genes for brain (C) were extracted from 11,468 targets and assembled in the order obtained from the results of the two-dimensional hierarchical cluster analysis. The results were drawn as a dendrogram based on the similarities of gene expression patterns of each sample. The *y*-axis of the dendrogram shown in (B) and (C) depicts the Euclid square distance as the dissimilarity coefficient, indicating the relationship between the samples. Red and blue indicate increases and decreases in the expression ratio, respectively.

clear clusters, corresponding to distinguishable gene expression patterns, were apparent, either in liver (Fig. 4B) or in brain (Fig. 4C). Gene expression patterns were very similar in all vaccine-treated samples.

Further, we tried to identify specific genes whose expression levels were changed following JE vaccine treatment.

However, no genes could be selected from the comparison between MBD- and VCD-treated groups. MBD and VCD treatment could not be distinguished by gene expression analyses, indicating equivalent characteristics of MBD and VCD.

## DISCUSSION

Comprehensive gene expression analysis is now an established approach to analyzing the effects of any manipulation on the whole transcriptome of living organisms. The genomic data associated with drug responses are expected to aid in the analysis of inter-individual variability and the tailoring of the administration of drugs to individuals to achieve maximal efficacy and minimum risk. The US Food and Drug Administration (FDA) now encourages voluntary genomic data submissions to the agency as part of new drug applications and biologics licensing applications (33). In this context, we have been trying to introduce DNA microarray analysis to the conventional quality control tests of the pertussis and influenza vaccines. The results of DNA microarray analysis correlated well with the results of conventional animal tests, and toxicity-related biomarkers were successfully extracted from the analysis (30–32). In the present study, we further applied this DNA microarray technology to analyze the biological reactivity of the JE vaccines (MBD and VCD). In liver and brain, the overall gene expression patterns were similar between MBD- and VCD-treated rats (Fig. 4), which was in accordance with the results obtained from the decreasing body weight test (Fig. 1) or the blood and serum tests (Figs. 2 and 3).

ADEM, an adverse reaction associated with JE vaccination, is thought to be a monophasic autoimmune disorder of the central nervous system, typically following a febrile infection or a vaccination (34). The precise mechanisms of ADEM have not been fully elucidated; however, recent studies suggested the involvement of inflammatory cytokines, such as tumor necrosis factor (TNF)-$\alpha$ and chemokines (35–37). Further, several genes associated with inflammation or immune responses, including Irf7, were up-regulated in JE virus-infected mouse brains (38,39). Therefore, inflammation above certain levels may be associated with adverse reactions to vaccines, that is, inflammation-related genes could be markers to detect contaminating toxicity that can cause adverse reactions. However, we found no significant changes in the expression levels of inflammatory genes between MBD- and VCD-treated rat tissues. We showed by using animal tests and comprehensive gene expression analysis that the two Japanese encephalitis vaccines, the existing MBD and the improved VCD vaccines, seemed to possess identical biological reactivity in rats.

To address concern about the reliability of the genomic data obtained from DNA microarray analysis, the FDA recently launched the MicroArray Quality Control (MAQC) project in anticipation of the regulatory submission of pharmacoinformatic and toxicoinformatic data in applications or supplements (33). The results of the MAQC project, showing interplatform reproducibility, were reported in 2006 (40–45). Subsequently, the follow-up MAQC-II project is progressing towards the development and the validation of genomic data in clinical applications. Similarly, in Japan, the Japan MicroArray Consortium (JMAC) for the standardization and the international harmonization of microarray platforms is ongoing and is coordinated with the FDA and the European Medical Agency (EMEA) (46). The efforts to achieve array platforms for the practical application of genomic data are being accelerated on a worldwide scale.

Although our experiments were limited with regard to the number of animals and vaccines examined, our DNA microarray technology was previously shown to be reproducible (30,32). The genomic data obtained in this study is, we believe, reliable. Recently, the VCD JE vaccine was licensed in Japan. It is desirable to accumulate gene expression profiles, especially data documenting the dynamics of inflammatory cytokines, in addition to generating animal testing data to enable a more reliable evaluation of the new JE vaccine.


## ACKNOWLEDGMENTS

The authors thank Keiko Furuhata and Momoka Tsuruhara for technical support.

This work was supported by Grants-in-Aid from the Ministry of Health, Labour and Welfare, Japan. The authors have no conflicting financial interests.


## REFERENCES


1. Gubler, D.J., Kuno, G. and Markoff, L. (2007): Flaviviruses. p. 1185–1190. *In* D.M. Knipe, P.M. Howley, D.E. Griffin, et al. (ed.), Fields Virology. 5th ed. vol. I. Lippincott Williams & Wilkins, Philadelphia.
2. World Health Organization (2006): Japanese encephalitis vaccines. Wkly. Epidemiol. Rec., 81, 331–340.
3. Halstead, S.B. and Jacobson, J. (2008): Japanese encephalitis vaccines. p. 311–352. *In* S.A. Plotkin, W.A. Orenstein, and P.A. Offit (ed.), Vaccines. 5th ed. Elsevier, New York.
4. Global Advisory Committee on Vaccine Safety, World Health Orgnization: Japanese encephalitis (JE) vaccines. Mouse brained-derived Japanese encephalitis (JE) vaccine. Online at <http://www.who.int/vaccine_safety/topics/japanese_encephalitis/mouse_brain_derived/en/>.
5. Hombach, J., Barrett, A.D., Cardosa, M.J., et al. (2005): Review on flavivirus vaccine development. Proceedings of a meeting jointly organised by the World Health Organization and the Thai Ministry of Public Health, 26–27 April 2004, Bangkok, Thailand. Vaccine, 23, 2689–2695.
6. Monath, T.P., Guirakhoo, F., Nichols, R., et al. (2003): Chimeric live, attenuated vaccine against Japanese encephalitis (ChimeriVax-JE): phase 2 clinical trials for safety and immunogenicity, effect of vaccine dose and schedule, and memory response to challenge with inactivated Japanese encephalitis antigen. J. Infect. Dis., 188, 1213–1230.
7. Kuzuhara, S., Nakamura, H., Hayashida, K., et al. (2003): Non-clinical and phase I clinical trials of a Vero cell-derived inactivated Japanese encephalitis vaccine. Vaccine, 21, 4519–4526.
8. Abe, M., Shiosaki, K., Hammar, L., et al. (2006): Immunological equivalence between mouse brain-derived and Vero cell-derived Japanese encephalitis vaccines. Virus Res., 121, 152–160.
9. Lyons, A., Kanesa-Thasan, N., Kuschner, R.A., et al. (2007): A Phase 2 study of a purified, inactivated virus vaccine to prevent Japanese encephalitis. Vaccine, 25, 3445–3453.
10. Tauber, E., Kollaritsch, H., Korinek, M., et al. (2007): Safety and immunogenicity of a Vero-cell-derived, inactivated Japanese encephalitis vaccine: a non-inferiority, phase III, randomised controlled trial. Lancet, 370, 1847–1853.
11. Pohl-Koppe, A., Burchett, S.K., Thiele, E.A., et al. (1998): Myelin basic protein reactive Th2 T cells are found in acute disseminated encephalomyelitis. J. Neuroimmunol., 91, 19–27.
12. Williams, D.T., Wang, L.F., Daniels, P.W., et al. (2000): Molecular characterization of the first Australian isolate of Japanese encephalitis virus, the FU strain. J. Gen. Virol., 81, 2471–2480.
13. Ritchie, S.A. and Rochester, W. (2001): Wind-blown mosquitoes and introduction of Japanese encephalitis into Australia. Emerg. Infect. Dis., 7, 900–903.
14. Barrett, P.N., Mundt, W., Kistner, O., et al. (2009): Vero cell platform in vaccine production: moving towards cell culture-based viral vaccines. Expert Rev. Vaccines, 8, 607–618.
15. Petricciani, J. and Sheets, R. (2008): An overview of animal cell substrates for biological products. Biologicals, 36, 359–362.
16. Montagnon, B., Vincent-Falquet, J.C. and Fanget, B. (1983): Thousand litre scale microcarrier culture of Vero cells for killed polio virus vaccine. Promising results. Dev. Biol. Stand., 55, 37–42.

17. Montagnon, B.J. (1989): Polio and rabies vaccines produced in continuous cell lines: a reality for Vero cell line. Dev. Biol. Stand., 70, 27–47.
18. Monath, T.P., Caldwell, J.R., Mundt, W., et al. (2004): ACAM2000 clonal Vero cell culture vaccinia virus (New York City Board of Health strain)–a second-generation smallpox vaccine for biological defense. Int. J. Infect. Dis., 8 Suppl 2, S31–44.
19. National Institute of Infectious Diseases, Japan (2006): Minimum Requirements for Biological Products. Online at <http://www.nih.go.jp/niid/MRBP/seibutsuki_english.pdf>.
20. Ito, E., Honma, R., Imai, J., et al. (2003): A tetraspanin-family protein, T-cell acute lymphoblastic leukemia-associated antigen 1, is induced by the Ewing's sarcoma-Wilms' tumor 1 fusion protein of desmoplastic small round-cell tumor. Am. J. Pathol., 163, 2165–2172.
21. Kobayashi, S., Ito, E., Honma, R., et al. (2004): Dynamic regulation of gene expression by the Flt-1 kinase and Matrigel in endothelial tubulogenesis. Genomics, 84, 185–192.
22. Kurokawa, M. (1984): Toxicity and toxicity testing of pertussis vaccine. Jpn. J. Med. Sci. Biol., 37, 41–81.
23. Horiuchi, Y., Takahashi, M., Konda, T., et al. (2001): Quality control of diphtheria tetanus acellular pertussis combined (DTaP) vaccines in Japan. Jpn. J. Infect. Dis., 54, 167–180.
24. Mizukami, T., Masumi, A., Momose, H., et al. (2009): An improved abnormal toxicity test by using reference vaccine-specific body weight curves and histopathological data for monitoring vaccine quality and safety in Japan. Biologicals, 37, 8–17.
25. Grifantini, R., Bartolini, E., Muzzi, A., et al. (2002): Previously unrecognized vaccine candidates against group B meningococcus identified by DNA microarrays. Nat. Biotechnol., 20, 914–921.
26. Yang, H.L., Zhu, Y.Z., Qin, J.H., et al. (2006): In silico and microarray-based genomic approaches to identifying potential vaccine candidates against *Leptospira interrogans*. BMC Genomics, 7, 293.
27. Shin, J., Wood, D., Robertson, J., et al. (2007): WHO informal consultation on the application of molecular methods to assure the quality, safety and efficacy of vaccines, Geneva, Switzerland, 7–8 April 2005. Biologicals, 35, 63–71.
28. Hamadeh, H.K., Bushel, P.R., Jayadev, S., et al. (2002): Gene expression analysis reveals chemical-specific profiles. Toxicol. Sci., 67, 219–231.
29. Ejiri, N., Katayama, K., Kiyosawa, N., et al. (2005): Microarray analysis on Phase II drug metabolizing enzymes expression in pregnant rats after treatment with pregnenolone-16alpha-carbonitrile or phenobarbital. Exp. Mol. Pathol., 79, 272–277.
30. Hamaguchi, I., Imai, J., Momose, H., et al. (2007): Two vaccine toxicity-related genes Agp and Hpx could prove useful for pertussis vaccine safety control. Vaccine, 25, 3355–3364.
31. Mizukami, T., Imai, J., Hamaguchi, I., et al. (2008): Application of DNA microarray technology to influenza A/Vietnam/1194/2004 (H5N1) vaccine safety evaluation. Vaccine, 26, 2270–2283.
32. Hamaguchi, I., Imai, J., Momose, H., et al. (2008): Application of quantitative gene expression analysis for pertussis vaccine safety control. Vaccine, 26, 4686–4696.
33. Frueh, F.W. (2006): Impact of microarray data quality on genomic data submissions to the FDA. Nat. Biotechnol., 24, 1105–1107.
34. Menge, T., Hemmer, B., Nessler, S., et al. (2005): Acute disseminated encephalomyelitis: an update. Arch. Neurol., 62, 1673–1680.
35. Ichiyama, T., Shoji, H., Kato, M., et al. (2002): Cerebrospinal fluid levels of cytokines and soluble tumour necrosis factor receptor in acute disseminated encephalomyelitis. Eur. J. Pediatr., 161, 133–137.
36. Kadhim, H., De Prez, C., Gazagnes, M.D., et al. (2003): In situ cytokine immune responses in acute disseminated encephalomyelitis: insights into pathophysiologic mechanisms. Hum. Pathol., 34, 293–297.
37. Franciotta, D., Zardini, E., Ravaglia, S., et al. (2006): Cytokines and chemokines in cerebrospinal fluid and serum of adult patients with acute disseminated encephalomyelitis. J. Neurol. Sci., 247, 202–207.
38. Saha, S., Sugumar, P., Bhandari, P., et al. (2006): Identification of Japanese encephalitis virus-inducible genes in mouse brain and characterization of GARG39/IFIT2 as a microtubule-associated protein. J. Gen. Virol., 87, 3285–3289.
39. Saxena, V., Mathur, A., Krishnani, N., et al. (2008): An insufficient anti-inflammatory cytokine response in mouse brain is associated with increased tissue pathology and viral load during Japanese encephalitis virus infection. Arch. Virol., 153, 283–292.
40. Canales, R.D., Luo, Y., Willey, J.C., et al. (2006): Evaluation of DNA microarray results with quantitative gene expression platforms. Nat. Biotechnol., 24, 1115–1122.
41. Shippy, R., Fulmer-Smentek, S., Jensen, R.V., et al. (2006): Using RNA sample titrations to assess microarray platform performance and normalization techniques. Nat. Biotechnol., 24, 1123–1131.
42. Tong, W., Lucas, A.B., Shippy, R., et al. (2006): Evaluation of external RNA controls for the assessment of microarray performance. Nat. Biotechnol., 24, 1132–1139.
43. Patterson, T.A., Lobenhofer, E.K., Fulmer-Smentek, S.B., et al. (2006): Performance comparison of one-color and two-color platforms within the MicroArray Quality Control (MAQC) project. Nat. Biotechnol., 24, 1140–1150.
44. Shi, L., Reid, L.H., Jones, W.D., et al. (2006): The MicroArray Quality Control (MAQC) project shows inter- and intraplatform reproducibility of gene expression measurements. Nat. Biotechnol., 24, 1151–1161.
45. Guo, L., Lobenhofer, E.K., Wang, C., et al. (2006): Rat toxicogenomic study reveals analytical consistency across microarray platforms. Nat. Biotechnol., 24, 1162–1169.
46. Imagawa, K., Ito, T. and Azuma, J. (2008): The present status and future perspectives on pharmacogenomics and toxicogenomics. Jpn. J. Clin. Pharmacol. Ther., 39, 61–67 (in Japanese).

Bioorganic & Medicinal Chemistry xxx (2010) xxx–xxx

Contents lists available at ScienceDirect

Bioorganic & Medicinal Chemistry

journal homepage: www.elsevier.com/locate/bmc

# Anti-influenza activity of phenethylphenylphthalimide analogs derived from thalidomide

Yuma Iwai [a,†], Hitoshi Takahashi [b,†], Dai Hatakeyama [a], Kazunori Motoshima [c], Minoru Ishikawa [c], Kazuyuki Sugita [c], Yuichi Hashimoto [c], Yuichi Harada [b], Shigeyuki Itamura [b], Takato Odagiri [b], Masato Tashiro [b], Yoshihisa Sei [d], Kentaro Yamaguchi [d], Takashi Kuzuhara [a,*]

[a] Laboratory of Biochemistry, Faculty of Pharmaceutical Sciences, Tokushima Bunri University, Yamashiro-cho, Tokushima 770-8514, Japan
[b] Center for Influenza Virus Research, National Institute of Infectious Diseases, Gakuen 4-7-1, Musashimurayama-shi, Tokyo 208-0011, Japan
[c] Institute of Molecular & Cellular Biosciences, The University of Tokyo, 1-1-1, Yayoi, Bunkyo-ku, Tokyo 113-0032, Japan
[d] Analytical Chemistry Laboratory, Faculty of Pharmaceutical Sciences at Kagawa Campus, Tokushima Bunri University, Sanuki-City, Kagawa 769-2193, Japan

ARTICLE INFO

*Article history:*
Received 21 April 2010
Revised 12 May 2010
Accepted 13 May 2010
Available online xxxx

*Keywords:*
Influenza
Thalidomide
RNA polymerase
Phenethylphenylphthalimide
Endonuclease

ABSTRACT

Swine-origin influenza A virus has caused pandemics throughout the world and influenza A is regarded as a serious global health issue. Hence, novel drugs that will target these viruses are very desirable. Influenza A expresses an RNA polymerase essential for its transcription and replication which comprises PA, PB1, and PB2 subunits. We identified potential novel anti-influenza agents from a screen of 34 synthesized phenethylphenylphthalimide analogs derived from thalidomide (PPT analogs). For this screen we used a PA endonuclease inhibition assay, a PB2 pathogenicity-determinant domain-binding assay, and an anti-influenza A virus assay. Three PPT analogs, PPT-65, PPT-66, and PPT-67, were found to both inhibit PA endonuclease activity and retard the growth of influenza A, suggesting a correlation between their activities. PPT-28 was also found to inhibit the growth of influenza A. These four analogs have a 3,4-dihydroxyphenethyl group in common. We also discuss the possibility that 3,4-dihydroxyphenethyl group flexibility may play an important functional role in PA endonuclease inhibition. Another analog harboring a dimethoxyphenethyl group, PPT-62, showed PB2 pathogenicity-determinant domain-binding activity, but did not inhibit the growth of the virus. Our present results indicate the utility of the PA endonuclease assay in the screening of anti-influenza drugs and are therefore useful for future strategies to develop novel anti-influenza A drugs and for mapping the function of the influenza A RNA polymerase subunits.



## 1. Introduction

Thalidomide, a hypnotic/sedative drug, was originally launched in the 1950s but was subsequently withdrawn from the market in the 1960s because of its teratogenic properties.[1,2] Thalidomide has been subsequently shown however to be useful in the treatment of Hansen's disease, multiple myeloma, cancer, rheumatoid arthritis, graft-versus-host diseases, and acquired immunodeficiency syndrome.[1–4] Pharmacologically, thalidomide has anti-cachexia, anti-inflammatory, anti-tumor-promoting, anti-angiogenic, tumor cell invasion-inhibiting, anti-viral, and hypoglycemic activities. Hence, thalidomide is a multi-target drug and is thought to be useful as a template in the development of other biologically active compounds. Indeed, Hashimoto and colleagues have previously developed various thalidomide analogs[2,3,5–7] and based on the target molecules have created tumor necrosis factor-production-regulating agents, cyclooxygenase inhibitors, nitric oxide synthase inhibitors, histone deacetylase inhibitors, anti-angiogenic agents, and tubulin polymerization inhibitors.[2,3,5–7] These researchers have also developed the structure of thalidomide based on its pharmacological effects and thereby produced androgen antagonists, progesterone antagonists, cell differentiation inducers, aminopeptidase inhibitors, thymidine phosphorylase inhibitors, μ-calpain inhibitors, α-glucosidase inhibitors, and nuclear liver X receptor antagonists.[2,3,5–7]

In 1918, an influenza A pandemic caused ten million deaths worldwide[8] and strategies to prevent any future expansions of this virus are therefore an important endeavor.[9,10] The avian H5N1 influenza A virus is highly pathogenic to humans[11] and the emer-

*Abbreviations:* PPT, phenethylphenylphthalimide; IPTG, isopropyl β-D-thiogalactopyranoside; ESI, electrospray ionization; MS, mass spectrometry; FT-ICRMS, Fourier transform ion cyclotron resonance mass spectrometer; MDCK, Madin–Darby canine kidney.

* Corresponding author. Tel.: +81 88 602 8477; fax: +81 88 655 3051.
*E-mail address:* kuzuhara@ph.bunri-u.ac.jp (T. Kuzuhara).

† These authors contributed equally to this work.

0968-0896/$ - see front matter © 2010 Elsevier Ltd. All rights reserved.
doi:10.1016/j.bmc.2010.05.035

gence of a new strain of this virus in 2009, the swine-origin A/H1N1 pdm influenza virus (SOIV), emphasizes this issue further as it has become a serious global health issue.[12] Although inhibitors of influenza A such as the neuraminidase-like compound oseltamivir are widely used as anti-viral drugs,[13,14] some adverse effects of these agents and also the emergence of viral strains that are resistant to these drugs have now been reported.[15–17]

For the prevention and control of influenza outbreaks, the development of novel anti-viral drugs that are not based on neuraminidase inhibition is now regarded as critical.[12] The influenza A genome consists of a segmented single stranded RNA (−) and its transcription and replication require the activity of a highly conserved RNA-dependent RNA polymerase.[18,19] This polymerase is essential for the influenza A virus to propagate and thus represents a very promising target for anti-viral drug development. The influenza A virus RNA-dependent RNA polymerase is composed of three subunits, PA, PB1, and PB2, and synthesizes viral mRNAs using short capped primers derived from host cellular pre-mRNAs cleaved by the viral endonuclease.[18,19] Yuan et al. and Dias et al. have shown that the N-terminal domain of the PA subunit contains the endonuclease active site and that this domain also harbors RNA/DNA endonuclease activity.[20–22] The PB2 subunit includes K627, which plays a role in the high pathogenicity and host range restriction of the virus.[23–26] We and others have elucidated the tertiary structure of the C-terminal domain (627 domain) of PB2 by X-ray crystallography and identified a unique loop and basic groove proximal to the K627 residue.[27,28] D701 N has also been shown to be associated with the viral pathogenicity levels and is also contained in this domain. Hence, we speculated that the PA endonuclease and PB2 627 domains would be very effective targets in the development of novel anti-influenza A drugs.

Our preliminary results in this regard suggested that phenethylphenylphthalimide (PPT) analogs derived from thalidomide are possible lead compounds (Supplementary Fig. 1) and we thus screened a further cohort of PPT analogs using a PA endonuclease inhibition assay, PB2 627 domain-binding assay and anti-influenza A virus assay. The results of these assays and also of our analysis of the structure–activity relationships of PPT analogs are described.

## 2. Results

### 2.1. Synthesis of PPT analogs

PPT derivatives were synthesized as previously described[29] in which diphenylethene derivatives were prepared as *E*/*Z* mixtures via a Wittig reaction of nitrobenzaldehyde with appropriately substituted benzyl ylide (Fig. 1A). After reduction of the nitro group and/or olefin moiety of the adducts, PPT derivatives were obtained by condensation with phthalic anhydride (Fig. 1A). We denoted our PPT analog series as PPT-*n* (*n* = sequential numbering from 1; Fig. 1B). We obtained 37 PPT analogs, three of which (PPT-108, -109, and -112) could not be dissolved in the aqueous assay buffer. We then adopted a strategy for developing a novel anti-influenza A drug which involved two initial in vitro screenings for the inhibition of PA endonuclease activity and a PB2 627 domain-binding assay. After these in vitro selections, we performed an anti-virus assay.

### 2.2. Inhibition of PA endonuclease by PPT analogs

In the in vitro PA endonuclease assay, we expressed and purified a recombinant PA endonuclease domain (1–220 residues) of the influenza A virus RNA polymerase as previously described.[22] The PA endonuclease domain digests M13mp18 ssDNA in vitro[22] (Fig. 2, lanes 1 and 2) and we examined which of our 34 soluble PPT analogs could inhibit this activity. In the assay, we incubated 0.1 μM of recombinant PA endonuclease domain with both 1 and 10 μM of each PPT analog (Fig. 1B). PPT-65 and PPT-66 significantly inhibited the digestion of M13mp18 at a dose of 10 μM (Fig. 2) and this is the first evidence that agents based on the thalidomide skeleton can inhibit the influenza A virus endonuclease. PPT-67 also showed weak inhibitory activity in this regard but none of the other 31 PPT analogs tested has any effects in the assay (Fig. 2). Interestingly, we found that PPT-65, PPT-66, and PPT-67 all contain a 3,4-dihydroxyphenethyl group (Fig. 1B), indicating that this moiety is important for the inhibition of PA endonuclease (Figs. 1B and 2). A detailed analysis of the structure–function relationships of the PPT analogs is provided later in Section 3.

### 2.3. Binding of PPT analogs to the PB2 627 domain

As another in vitro selection, we next screened for PB2 627 domain (residues 535–759)-binding factors among PPT analogs. This domain has been reported to be associated with viral pathogenicity and host range restriction,[25–28] and we speculated that it would play an important role and that any chemical that bound to this domain would have anti-viral effects. We established an assay system to detect the PB2 627 domain protein by ESI-MS.[30,31] In this analysis, molecular weights are presented as a number divided by the charge number, which in the case of the PB2 627 domain is 25146. As shown in Figure 3A, peaks with sodium adducts appeared with the mass to charge (*m*/*z*), which corresponds to the molecular weight of the PB2 627 domain (Fig. 2A). We thus concluded that these peaks are derived from an intact PB2 627 domain protein. We next mixed and analyzed 1–3 μM of PB2 627 domain protein with 50 μM of each PPT analog to detect whether binding occurred. When PB2 627 domain mixed with PPT-62 (Fig. 3F), additional peaks other than the PB2 627 domain were appeared. The differences of *m*/*z* values between additional peaks and those derived from PB2 627 domain were 43.0 and 42.7 (Fig. 3F). When multiplied by nine, these values become 387 and 384 which are almost same as the molecular weight of PPT-62 (387). In case of the other charge, especially e = 8, shifted peaks were also observed (Supplementary Fig. 2). This indicates that PPT-62 directly associates with the PB2 627 domain. No binding was observed for several other PPT analogs (Fig. 3B–G), indicating that the association of PPT-62 and PB2 627 is specific. Two kinds of bound form of PB2 627 domain, (PB2 627 domain + PPT-62) and (PB2 627 domain + two PPT-62), were observed indicating that two molecules of PPT-62 bind to this domain. This may be because two PPT-62 molecules interact with each other via π–π bonding because this chemical contains an aromatic ring.

### 2.4. Inhibition of influenza A by PPT analogs

We performed an influenza A virus assay in a cell culture system for the four PPT analogs that selected by these two in vitro assays (PPT-62, -65, -66, and -67), and also include one further PPT analog (PPT-28) containing a 3,4-dihydroxyphenethyl group, and additional analogs (PPT-68 and -125) for comparison. MDCK cells undergo cytopathy following infection by influenza A in culture and we used this system to examine whether our selected PPT analogs could inhibit growth of this virus. Various concentrations (0.63–80 μM) of each PPT analog and 100 $TCID_{50}$ (50% of the infectious dose) of influenza A virus were premixed, and then added to the culture medium of the MDCK cells. We performed this assay three times and thereby determined the viability of the MDCK cells (Fig. 4). DMSO alone did not inhibit the viral growth whereas PPT-65 and -66 did so at a dose of around 40 μM (Fig. 4). PPT-67 also exerted these effects, but was more toxic to the cells (Supplementary Fig. 3). This is the first evidence that compounds with a

Please cite this article in press as: Iwai, Y.; et al. *Bioorg. Med. Chem.* (2010), doi:10.1016/j.bmc.2010.05.035

A

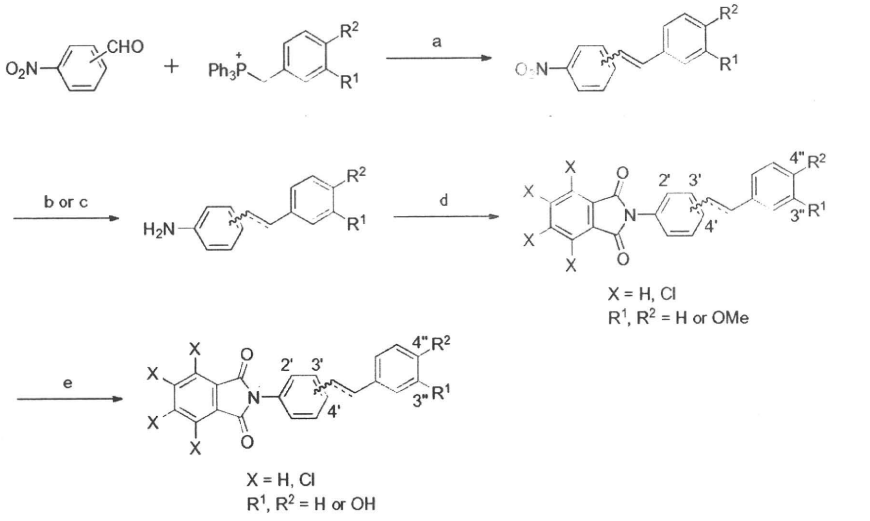


B

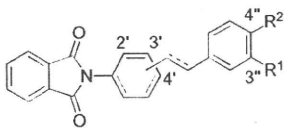

| Compound | position | single (s) or double bond (d) | $R^1$ | $R^2$ |
|---|---|---|---|---|
| **PPT2P** | 2' | s | H | H |
| **PPT62** | 2' | s | OMe | OMe |
| **PPT65** | 2' | s | OH | OH |
| **PPT63** | 3' | s | OMe | OMe |
| **PPT66** | 3' | s | OH | OH |
| **PPT21** | 4' | s | H | H |
| **PPT32** | 4' | s | OMe | OMe |
| **PPT108** | 4' | d | H | H |
| **PPT113** | 4' | d | OH | OH |
| **PPT121** | 4' | s | OMe | H |
| **PPT123** | 4' | s | H | OMe |
| **PPT125** | 4' | s | OH | H |
| **PPT137** | 4' | s | H | OH |

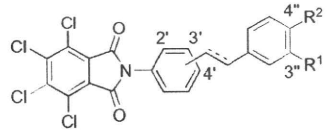

| Compound | position | single (s) or double bond (d) | $R^1$ | $R^2$ |
|---|---|---|---|---|
| **PPT43** | 2' | s | H | H |
| **PPT59** | 2' | s | OMe | OMe |
| **PPT67** | 2' | s | OH | OH |
| **PPT61** | 3' | s | H | H |
| **PPT60** | 3' | s | OMe | OMe |
| **PPT68** | 3' | s | OH | OH |
| **PPT22** | 4' | s | H | H |
| **PPT27** | 4' | s | OMe | OMe |
| **PPT28** | 4' | s | OH | OH |
| **PPT84** | 3' | d | H | H |
| **PPT95** | 3' | d | OMe | OMe |
| **PPT97** | 3' | d | OH | OH |
| **PPT109** | 4' | d | H | H |
| **PPT112** | 4' | d | OMe | OMe |
| **PPT91** | 3' | s | OMe | H |
| **PPT80** | 3' | s | H | OMe |
| **PPT94** | 3' | s | OH | H |
| **PPT85** | 3' | s | H | OH |
| **PPT122** | 4' | s | OMe | H |
| **PPT124** | 4' | s | H | OMe |
| **PPT136** | 4' | s | OH | H |
| **PPT138** | 4' | s | H | OH |

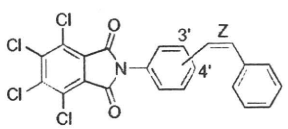

| Compound | position |
|---|---|
| **PPT86** | 3' |
| **PPT87** | 4' |

**Figure 1.** (A) Scheme of the chemical synthesis of PPT analogs. Reagents and conditions: (a) $K_2CO_3$, 18-crown-6, $CH_2Cl_2$, reflux; (b) $H_2$, 10%, Pd/C, EtOAc, rt; (c) $SnCl_2{\cdot}2H_2O$, EtOAc, reflux; (d) phthalic anhydride or tetrachlorophthalic anhydride, neat, 200 °C; (e) $BBr_3$, $CH_2Cl_2$, 0 °C. (B) Chemical structures of the synthesized PPT analogs screened for anti-influenza A activities.

phthalimide skeleton derived from thalidomide possess anti-influenza A virus activity. PPT-62, -68, and -125 did not inhibit the viral growth (Fig. 4) nor inhibit PA endonuclease activity (Fig. 2). Hence, a correlation exists between the inhibition of PA endonuclease and inhibition of influenza A. Interestingly, we also found that PPT-28, which contains a 3,4-dihydroxyphenethyl group, inhibits the influenza virus but not via the targeting of the PA endonuclease. Table 1 lists the $EC_{50}$ and $CC_{50}$ values for these analogs which were calculated from the data shown in Figure 4. The average $EC_{50}$ for PPT-28, -65, and -66 was 24, 48, and 26 μM, and the $CC_{50}$ of PPT-28 and -65 was above 80 μM, respectively. These compounds are therefore putative candidate anti-influenza A drugs themselves and may also have utility as seeds for the development of such agents.

## 3. Discussion

We demonstrate that three PPT analogs, PPT-65, PPT-66, and PPT-67, inhibit PA endonuclease and the viral growth. Significantly,

Please cite this article in press as: Iwai, Y.; et al. *Bioorg. Med. Chem.* (2010), doi:10.1016/j.bmc.2010.05.035

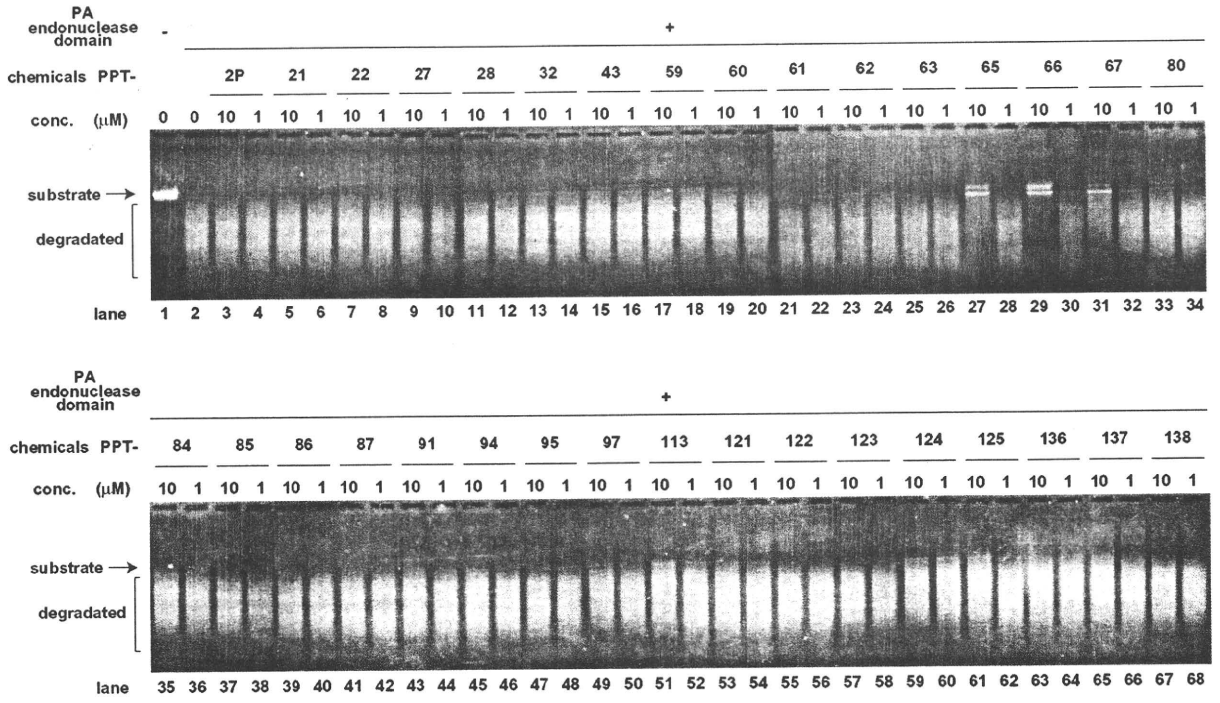


**Figure 2.** Screening of PPT analogs for anti-influenza A activity using a PA endonuclease assay. Effects of various PPT analogs upon the endonuclease activity of the N-terminal domain of the PA subunit of influenza A virus RNA-dependent RNA polymerase. The recombinant N-terminal domain of PA was added to each reaction at 0.35 μg/100 μl. A zero control (no PA domain added) was also assayed. PPT analogs were added at 1 or 10 μM and M13mp18 was used as the substrate.

all of these analogs contain a 3,4-dihydroxyphenethyl group at the *ortho* or *meta* position of the *N*-phenyl moiety (Fig. 1B). The PPT analogs possessing methoxyphenethyl group(s) (PPT-27, -32, -59, -60, -62, -63, -80, -91, -95, -121, -122, -123, and -124), a monohydroxyphenethyl group (PPT-85, -94, -125, -136, -137, and -138) or an unsubstituted phenethyl group (PPT-21, -22, -43, -61, -84, -86, -87 and PPT2P) (Fig. 1B) did not inhibit PA endonuclease activity (Fig. 2). This suggests a central functional role of the 3,4-dihydroxyphenethyl moiety for this inhibition. Previously, we have reported that catechins[32] can inhibit PA endonuclease[22] and it has been shown also that these molecules have anti-influenza activity.[33] Significantly, the catechins also contain a 3,4-dihydroxyphenyl group (Supplementary Fig. 4), confirming that this moiety plays a role in the inhibition of PA endonuclease and in suppressing the growth of influenza (Fig. 5).

PPT-28 possesses a 3,4-dihydroxyphenethyl group at the *para* position (Fig. 1B) and does not inhibit PA endonuclease (Fig. 2), indicating that introduction of 3,4-dihydroxyphenethyl group into the '*ortho* or *meta*' position of the *N*-phenyl moiety be critical for this activity. Moreover, conversion of the 3,4-dihydroxyphenethyl group to a 3,4-dihydroxycinnamyl group, that is, as seen for PPT-97 and -113 (Fig. 1B), results in the loss of PA endonuclease-inhibitory activity (Fig. 2), also indicating the importance of the flexible 3,4-dihydroxyphenethyl group for this process. A freely rotating 3,4-dihydroxyphenyl group might also play an important functional role in this process. In combination with the importance of the position (*ortho* or *meta* of the *N*-phenyl moiety) at which the 3,4-dihydroxyphenethyl group is introduced, the spatial position of the two hydroxyl groups of the 3,4-dihydroxyphenethyl moiety in the molecule seem also to be critical for this activity. PPT-68 has a 3,4-dihydroxyphenethyl group but shows little or no inhibition of PA endonuclease (data not shown). We suggest therefore that the four chloride groups introduced into the phthalimide moiety inhibit or weaken this activity as PPT-67 also possesses a tetrachlorophthalimide group and shows weaker inhibition than PPT-65 or PPT-66 (Figs. 1 and 2). Although we have not yet investigated other functional groups derived from catechin, that is, 3,4,5-trihydroxyphenethyl and/or 3,5-dihydroxyphenethyl groups among others, our current results indicate that the development of chemicals with a 3,4-dihydroxyphenethyl group will likely produce more effective PA endonuclease inhibitors and better anti-influenza A drugs.

PPT-62 binds to the PB2 pathogenicity-determining 627 domain and harbors a dimethoxyphenethyl group (Figs. 1B and 3). In contrast, PPT-21 and PPT-43 do not possess a dimethoxyphenethyl group (Fig. 1B) and did not show binding to this domain (Fig. 3). PPT-62 is very similar to PPT-67 except for a methoxy group (Fig. 1B) but as PPT-67 binds only weakly to the PB2 627 domain (Fig. 3), the dimethoxy group of PPT-62 is likely to be important for this domain-binding. PPT-59 is identical to PPT-62 other than four additional chlorides (Fig. 1B) and also binds only weakly to the PB2 627 domain (Fig. 3), suggesting that these chlorides inhibit this binding. Based on these results, the development of compounds possessing a dimethoxyphenethyl group will likely lead to the production of drugs with a higher affinity for the PB2 627 domain.

Our current data show that PPT analogs can be used as tools to investigate the functional roles of influenza A virus RNA polymerase domains. Based on our results (summarized in Fig. 6), the PB2 pathogenicity-determinant domain may have a regulatory function rather than an essential one. Also, the correlation between the inhibition of PA endonuclease and suppression of the influenza A virus confirmed the importance of this enzyme for viral growth. Our results also indicate that the PA endonuclease assay is a useful screening tool for novel anti-influenza A drugs as the information obtained correlates well with virus

Please cite this article in press as: Iwai, Y.; et al. *Bioorg. Med. Chem.* (2010), doi:10.1016/j.bmc.2010.05.035

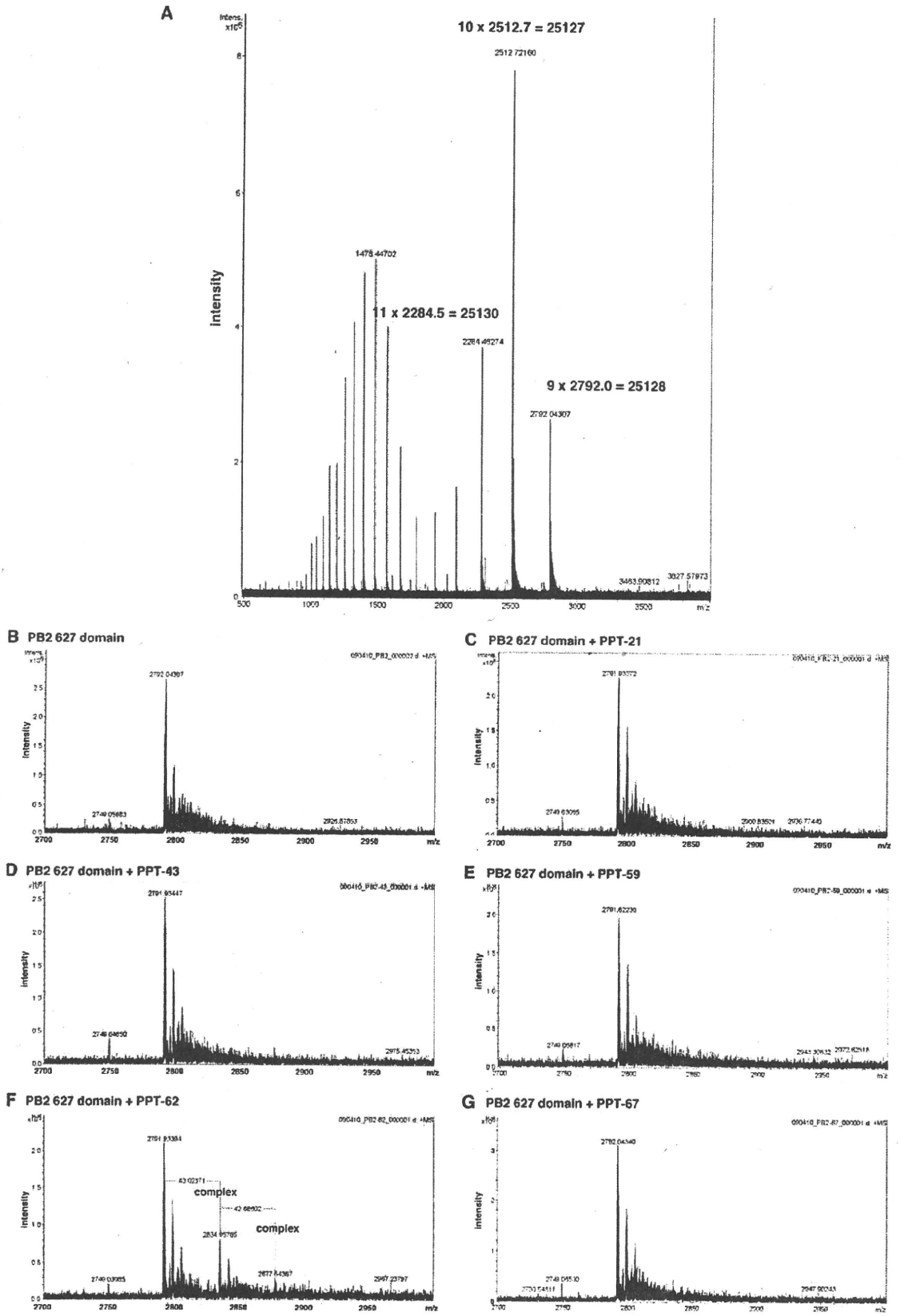


**Figure 3.** (A) Establishment of a detection system for factors that bind to the PB2 627 domain protein using FT-ICRMS. Vertical axis shows the intensity of the protein peaks. The horizontal axis indicates the *m/z* values. (B–G) Binding of PPT analogs to the PB2 627 domain. Direct binding analysis of PPT analogs to the PB2 627 domain using FT-ICRMS. The PB2 627 domain and PPT analogs were mixed and applied to FT-ICRMS. The vertical axis shows the intensity of the peaks. The horizontal axis indicates the *m/z* values. (B) PB2 627 domain only. The PB2 627 domain was also incubated with (C) PPT-21; (D) PPT-43; (E) PPT-59; (F) PPT-62 and (G) PPT-67.

Please cite this article in press as: Iwai, Y.; et al. *Bioorg. Med. Chem.* (2010), doi:10.1016/j.bmc.2010.05.035

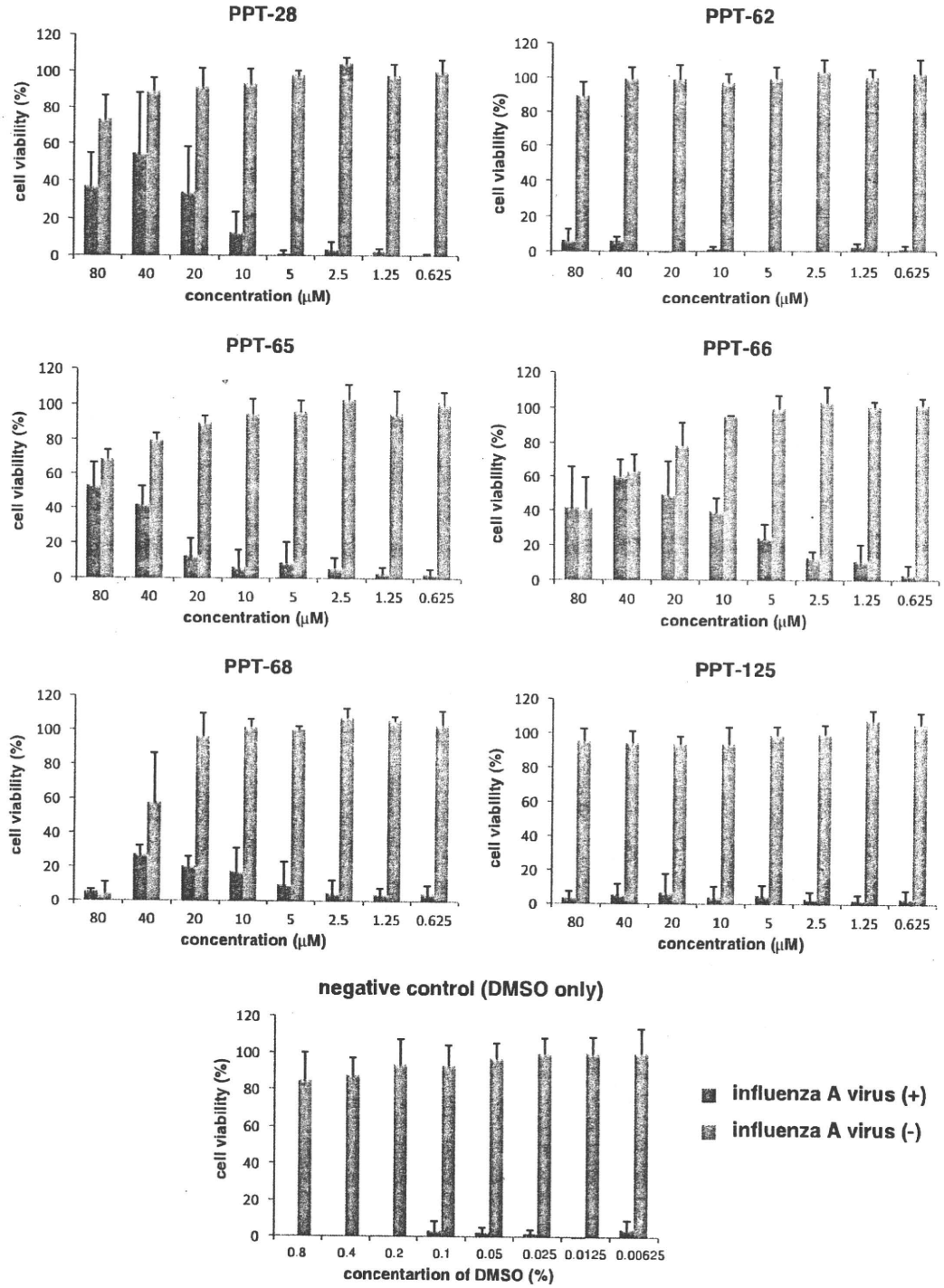


**Figure 4.** Inhibition of influenza A viral growth by PPT analogs. MDCK cells were treated with (red bar) or without (blue bar) influenza A virus. The cells were then treated with various concentrations of PPT analogs (0.63–80 μM), some of which suppressed viral-induced cell death. DMSO was used as the PPT solvent. The vertical and horizontal axes indicate cell viability (%) and the concentration of PPT analogs, respectively. Experiments were performed in triplicate, and the average values with standard deviations are indicated.

growth and this method is easier and thus more convenient to perform than other screening approaches using the virus itself. The effective doses of PPT analogs are high at present, but as the tertiary structures of the PA endonuclease and PB2 627 domains have already been determined,[20,21,27,28] docking simulations in silico[34] can be used for the further development and optimization of these compounds. We conclude finally that the chemical and biochemical information presented herein will be

Please cite this article in press as: Iwai, Y.; et al. *Bioorg. Med. Chem.* (2010), doi:10.1016/j.bmc.2010.05.035

**Table 1**
$EC_{50}$ and $CC_{50}$ values for the anti-influenza A activities of the indicated PPT analogs

| Virus (μM) | DMSO | | PPT-28 | | PPT-62 | | PPT-65 | | PPT-66 | | PPT-68 | | PPT-125 | |
|---|---|---|---|---|---|---|---|---|---|---|---|---|---|---|
| | (+) $EC_{50}$ | (−) $CC_{50}$ | (+) $EC_{50}$ | (−) $CC_{50}$ | (+) $EC_{50}$ | (−) $CC_{50}$ | (+) $EC_{50}$ | (−) $CC_{50}$ | (+) $EC_{50}$ | (−) $CC_{50}$ | (+) $EC_{50}$ | (−) $CC_{50}$ | (+) $EC_{50}$ | (−) $CC_{50}$ |
| 1st | >80 | >80 | 30 | >80 | >80 | >80 | 60 | >80 | 28 | >80 | >80 | 62 | >80 | >80 |
| 2nd | >80 | >80 | 25 | >80 | >80 | >80 | 37 | >80 | 11 | 48 | >80 | 34 | >80 | >80 |
| 3rd | >80 | >80 | 16 | >80 | >80 | >80 | >80[a] | >80 | 40 | 57 | >80 | 37 | >80 | >80 |
| Average | >80 | >80 | 24 | >80 | >80 | >80 | 48[b] | >80 | 26 | nd | >80 | 44 | >80 | >80 |

The $EC_{50}$ and $CC_{50}$ (μM) values were estimated from a dose-dependent curve in Figure 4.
nd, not determined.
[a] The $EC_{40}$ was around 50 (μM). The $EC_{50}$ was not estimated due to the low viability of the cells exposed to this higher dose. The shapes of the curves calculated for the three experiments are similar as shown in Supplementary Figure 5.
[b] Average was calculated from the first and second experiments in this case. See Supplementary Figure 5.

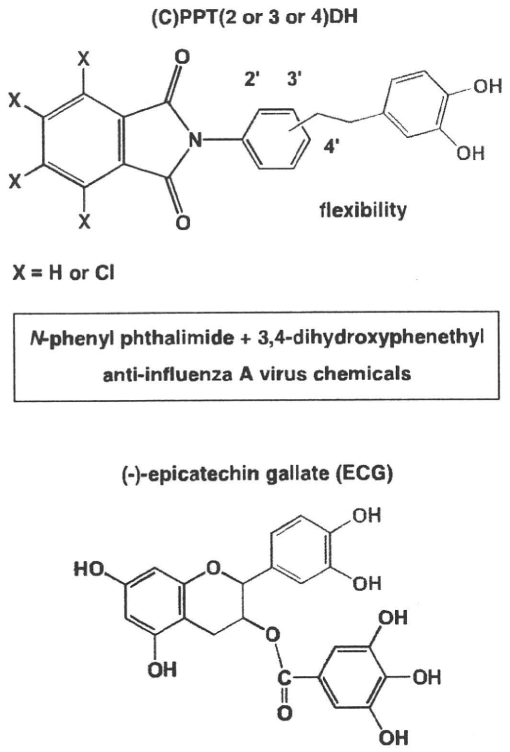


**Figure 5.** Consensus structure for the PPT analogs possessing anti-influenza A activity. The 3,4-dihydroxyphenyl group is characteristic of catechin molecules (shown as red) which also inhibit the influenza virus.

very useful for the future development of novel drugs against the influenza A virus.

## 4. Experimental

### 4.1. Synthesis of PPT analogs

Synthesis of the PPT analogs is described in the text and depicted also in Figure 1A. Their chemical structures are depicted in Figure 1B.

#### 4.1.1. *N*-(2-(2-Phenylethyl)phenyl)phthalimide: PPT2P

Mp 90.8–91.2 °C. $^1$H NMR (500 MHz, $CDCl_3$) $\delta$: 7.94–7.98 (m, 2H), 7.78–7.82 (m, 2H), 7.40 (dt, 1H, $J$ = 7.5, 1.5 Hz), 7.33–7.37 (m 2H), 7.16–7.22 (m, 3H), 7.10–7.15 (m 1H), 7.04–7.08 (m, 2H), 2.78–2.89 (m, 4H). Anal. Calcd for $C_{22}H_{17}NO_2$: C, 80.71; H, 5.23; N, 4.28. Found: C, 80.85; H, 5.36; N, 4.20.

#### 4.1.2. *N*-(4-(2-Phenylethyl)phenyl)phthalimide: PPT-21

Mp 216.5–218.0 °C. $^1$H NMR (500 MHz, $CDCl_3$) $\delta$: 7.96 (dd, 2H, $J$ = 5.5, 3.1 Hz), 7.50 (dd, 2H, $J$ = 5.5, 3.1 Hz), 7.36–7.29 (m, 6H), 7.23–7.19 (m, 3H), 3.01–2.94 (m, 4H). FAB-MS $m/z$: 327 $[M]^+$, 328 $[M+H]^+$. Anal. Calcd for $C_{22}H_{17}NO_2$: C, 80.71; H, 5.23; N, 4.28. Found: C, 80.71; H, 5.53; N, 4.27.

#### 4.1.3. 4,5,6,7-Tetrachloro-*N*-[4-(2-phenylethyl)phenyl]phthalimide: PPT-22

Mp 222.0–223.0 °C. $^1$H NMR (500 MHz, $CDCl_3$) $\delta$: 7.33–7.28 (m, 6H), 7.22–7.19 (m, 3H), 3.00–2.98 (m, 2H), 2.97–2.94 (m, 2H). FAB-MS $m/z$: 463 $[M]^+$, 464 $[M+H]^+$, 465 $[M+2]^+$, 466 $[M+3]^+$, 467 $[M+4]^+$, 468 $[M+5]^+$. Anal. Calcd for $C_{22}H_{13}Cl_4NO_2$: C, 56.81; H, 2.82; N, 3.01. Found: C, 56.85; H, 3.02; N, 2.94.

#### 4.1.4. 4,5,6,7-Tetrachloro-*N*-{4-[2-(3,4-dimethoxyphenyl)ethyl]phenyl}phthalimide: PPT-27

Mp 220.0–221.5 °C. $^1$H NMR (500 MHz, $CDCl_3$) $\delta$: 7.28 (s, 4H), 6.78 (d, 1H, $J$ = 8.5 Hz), 6.71 (dd, 1H, $J$ = 8.5, 1.8 Hz), 6.62 (d, 1H, $J$ = 1.8 Hz), 3.85 (s, 3H), 3.82 (s, 3H), 2.96–2.93 (m, 2H), 2.90–2.87 (m, 2H). FAB-MS $m/z$: 523 $[M]^+$, 524 $[M+H]^+$, 525 $[M+2]^+$, 526 $[M+3]^+$, 527 $[M+4]^+$, 528 $[M+5]^+$. HRMS (FAB) calcd for $C_{24}H_{17}Cl_4NO_4$ 522.9912; found: 522.9929 $(M)^+$.

#### 4.1.5. 4,5,6,7-Tetrachloro-*N*-{4-[2-(3,4-dihydroxyphenyl)ethyl]phenyl}phthalimide: PPT-28

Mp 260.0–263.0 °C. $^1$H NMR (500 MHz, DMSO-$d_6$) $\delta$: 8.70 (s, 1H), 8.62 (s, 1H), 7.38 (d, 2H, $J$ = 8.5 Hz), 7.30 (d, 2H, $J$ = 8.5 Hz), 6.64 (d, 1H, $J$ = 2.1 Hz), 6.62 (d, 1H, $J$ = 7.9 Hz), 6.47 (dd, 1H, $J$ = 7.9, 2.1 Hz), 2.88–2.85 (m, 2H), 2.75–2.72 (m, 2H). FAB-MS $m/z$: 495 $[M]^+$, 496 $[M+H]^+$, 497 $[M+2]^+$, 498 $[M+3]^+$, 499 $[M+4]^+$, 500 $[M+5]^+$. Anal. Calcd for $C_{22}H_{13}Cl_4NO_4 \cdot 1/3H_2O$: C, 52.52; H, 2.74; N, 2.78. Found: C, 52.47; H, 2.85; N, 2.51.

#### 4.1.6. *N*-{4-[2-(3,4-Dimethoxyphenyl)ethyl]phenyl}phthalimide: PPT-32

Mp 180.0–181.0 °C. $^1$H NMR (500 MHz, $CDCl_3$) $\delta$: 7.94 (dd, 2H, $J$ = 5.5, 3.1 Hz), 7.77 (dd, 2H, $J$ = 5.5, 3.1 Hz), 7.33–7.28 (m, 4H), 6.79 (d, 1H, $J$ = 7.9 Hz), 6.73 (dd, 1H, $J$ = 7.9, 1.8 Hz), 6.63 (d, 1H, $J$ = 1.8 Hz), 3.85 (s, 3H), 3.82 (s, 3H), 2.95–2.92 (m, 2H), 2.90–2.87 (m, 2H). FAB-MS $m/z$: 387 $[M]^+$, 388 $[M+H]^+$. Anal. Calcd for $C_{24}H_{21}NO_4 \cdot 1/5H_2O$: C, 73.72; H, 5.52; N, 3.58. Found: C, 73.98; H, 5.44; N, 3.64.

#### 4.1.7. 4,5,6,7-Tetrachloro-*N*-[2-(2-phenylethyl)phenyl]phthalimide: PPT-43

Mp 148.0–149.0 °C. $^1$H NMR (500 MHz, $CDCl_3$) $\delta$: 7.42–7.39 (m, 1H), 7.35–7.32 (m, 2H), 7.19–7.16 (m, 2H), 7.14–7.09 (m, 2H), 7.06 (d, 2H, $J$ = 6.7 Hz), 2.87–2.84 (m, 2H), 2.78–2.75 (m, 2H). FAB-MS $m/z$: 463 $[M]^+$, 464 $[M+H]^+$, 465 $[M+2]^+$, 466 $[M+3]^+$, 467 $[M+4]^+$,

Please cite this article in press as: Iwai, Y.; et al. *Bioorg. Med. Chem.* (2010), doi:10.1016/j.bmc.2010.05.035

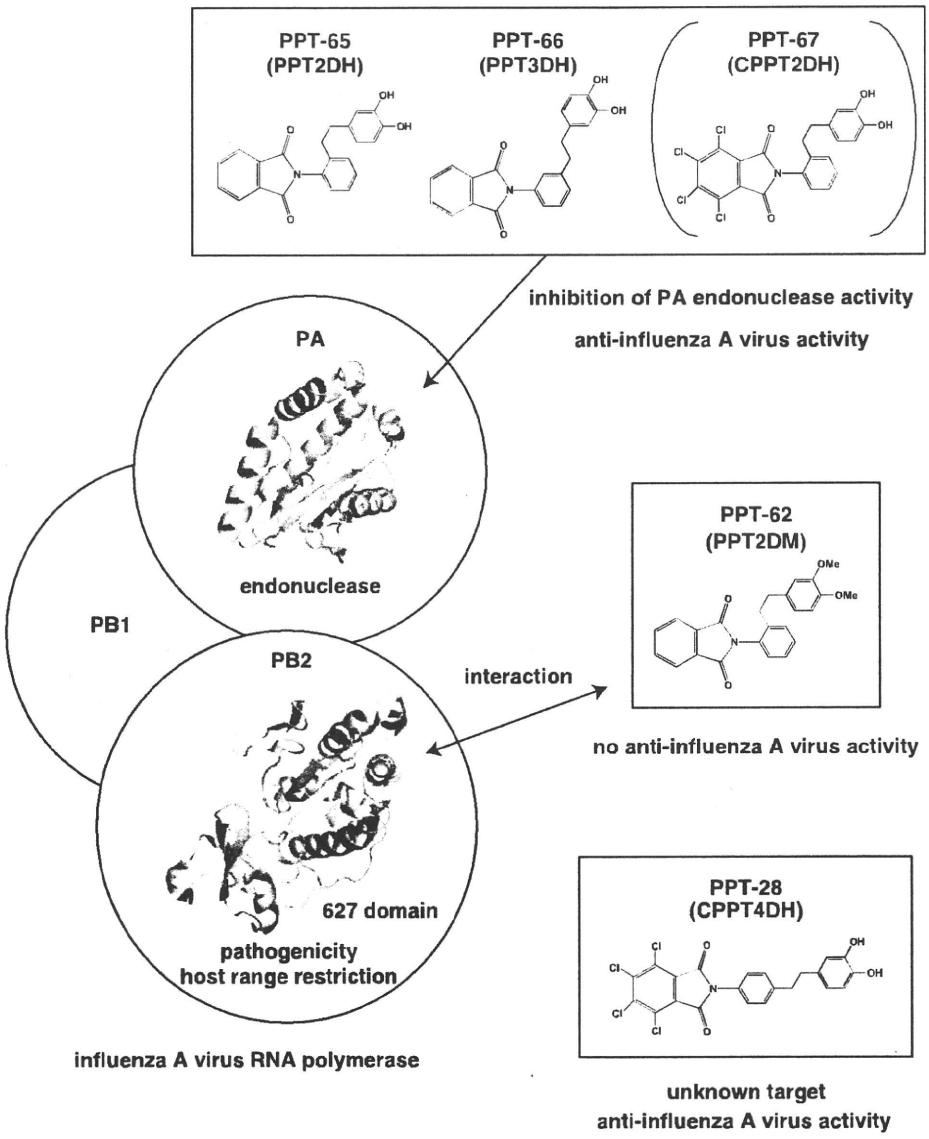


**Figure 6.** The functional domains of influenza A virus RNA polymerase mapped with respect to their interaction with the PPT analogs. PPT-65, -66, and -67 inhibit PA endonuclease activity and have anti-influenza A virus activity. PPT-62 binds to the PB2 pathogenicity-determinant 627 domain. PPT-28 has anti-influenza A virus activity. Structure–function relationship analysis indicates that the 3,4-dihydroxyphenethyl group is important for the anti-influenza A activity of these analogs.

468 $[M+5]^+$. Anal. Calcd for $C_{22}H_{13}Cl_4NO_2$: C, 56.81; H, 2.82; N, 3.01. Found: C, 56.67; H, 2.92; N, 2.94.

#### 4.1.8. 4,5,6,7-Tetrachloro-*N*-{2-[2-(3, 4-dimethoxyphenyl)ethyl] phenyl}phthalimide: PPT-59

Mp 157.0–158.0 °C. $^1$H NMR (500 MHz, $CDCl_3$) $\delta$: 7.41 (td, 1H, $J$ = 7.9, 1.8 Hz), 7.35 (td, 1H, $J$ = 7.9, 1.8 Hz), 7.32 (dd, 1H, $J$ = 7.3, 1.8 Hz), 7.15 (dd, 1H, $J$ = 7.9, 1.8 Hz), 6.68 (d, 1H, $J$ = 7.9 Hz), 6.61 (dd, 1H, $J$ = 7.9, 1.8 Hz), 6.53 (d, 1H, $J$ = 1.8 Hz), 3.81 (s, 3H), 3.75 (s, 3H), 2.80 (s, 4H). FAB-MS $m/z$: 523 $[M]^+$, 524 $[M+H]^+$, 525 $[M+2]^+$, 526 $[M+3]^+$, 527 $[M+4]^+$, 528 $[M+5]^+$. Anal. Calcd for $C_{24}H_{17}Cl_4NO_4$: C, 54.88; H, 3.26; N, 2.67. Found: C, 54.63; H, 3.37; N, 2.54.

#### 4.1.9. 4,5,6,7-Tetrachloro-*N*-{3-[2-(3,4-dimethoxyphenyl)ethyl] phenyl}phthalimide: PPT-60

Mp 166.0–167.0 °C. $^1$H NMR (500 MHz, $CDCl_3$) $\delta$: 7.43–7.39 (m, 1H), 7.24–7.20 (m, 3H), 6.79 (d, 1H, $J$ = 7.9 Hz), 6.71 (dd, 1H, $J$ = 7.9, 1.8 Hz), 6.64 (d, 1H, $J$ = 1.8 Hz), 3.86 (s, 3H), 3.83 (s, 3H), 2.97–2.94 (m, 2H), 2.91–2.88 (m, 2H). FAB-MS $m/z$: 523 $[M]^+$, 524 $[M+H]^+$, 525 $[M+2]^+$, 526 $[M+3]^+$, 527 $[M+4]^+$, 528 $[M+5]^+$. Anal. Calcd for $C_{24}H_{17}Cl_4NO_4 \cdot 1/4H_2O$: C, 54.42; H, 3.33; N, 2.64. Found: C, 54.49; H, 3.36; N, 2.61.

#### 4.1.10. 4,5,6,7-Tetrachloro-*N*-[3-(2-phenylethyl)phenyl]phthalimide: PPT-61

Mp 187.0–187.5 °C. $^1$H NMR (500 MHz, $CDCl_3$) $\delta$: 7.42 (t, 1H, $J$ = 7.9 Hz), 7.29 (t, 2H, $J$ = 7.9 Hz), 7.26–7.25 (m, 1H), 7.24 (dd, 2H, $J$ = 7.9, 1.8 Hz), 7.20 (dd, 1H, $J$ = 7.9, 1.2 Hz), 7.19 (d, 2H, $J$ = 7.9 Hz), 3.00–2.97 (m, 2H), 2.96–2.94 (m, 2H). FAB-MS $m/z$: 463 $[M]^+$, 464 $[M+H]^+$, 465 $[M+2]^+$, 466 $[M+3]^+$, 467 $[M+4]^+$, 468 $[M+5]^+$. Anal. Calcd for $C_{22}H_{13}Cl_4NO_2$: C, 56.81; H, 2.82; N, 3.01. Found: C, 56.66; H, 2.91; N, 2.95.

#### 4.1.11. *N*-{2-[2-(3,4-Dimethoxyphenyl)ethyl]phenyl}phthalimide: PPT-62

Mp 103.0–105.0 °C. $^1$H NMR (500 MHz, $CDCl_3$) $\delta$: 7.95 (dd, 2H, $J$ = 5.5, 3.1 Hz), 7.80 (dd, 2H, $J$ = 5.5, 3.1 Hz), 7.41–7.37 (m, 1H),

Please cite this article in press as: Iwai, Y.; et al. *Bioorg. Med. Chem.* (2010), doi:10.1016/j.bmc.2010.05.035

7.37–7.33 (m, 1H), 7.31 (dd, 1H, $J$ = 7.3, 1.8 Hz), 7.20 (dd, 1H, $J$ = 7.3, 1.8 Hz), 6.69 (d, 1H, $J$ = 7.9 Hz), 6.59 (dd, 1H, $J$ = 7.9, 1.8 Hz), 6.50 (d, 1H, $J$ = 1.8 Hz), 3.80 (s, 3H), 3.68 (s, 3H), 2.79 (s, 4H). FAB-MS $m/z$: 387 $[M]^+$, 388 $[M+H]^+$. Anal. Calcd for $C_{24}H_{21}NO_4$: C, 74.40; H, 5.46; N, 3.62. Found: C, 74.34; H, 5.59; N, 3.55.

#### 4.1.12. *N*-{3-[2-(3,4-Dimethoxyphenyl)ethyl]phenyl} phthalimide: PPT-63

Mp 132.5–133.5 °C. $^1$H NMR (500 MHz, $CDCl_3$) $\delta$: 7.96 (dd, 2H, $J$ = 5.5, 3.1 Hz), 7.80 (dd, 2H, $J$ = 5.5, 3.1 Hz), 7.43–7.39 (m, 1H), 7.28–7.26 (m, 2H), 7.19 (d, 1H, $J$ = 7.3 Hz), 6.80 (d, 1H, $J$ = 7.9 Hz), 6.73 (dd, 1H, $J$ = 7.9, 1.8 Hz), 6.65 (d, 1H, $J$ = 1.8 Hz), 3.85 (s, 3H), 3.83 (s, 3H), 2.99–2.95 (m, 2H), 2.93–2.89 (m, 2H). FAB-MS $m/z$: 387 $[M]^+$, 388 $[M+H]^+$. Anal. Calcd for $C_{24}H_{21}NO_4$: C, 74.40; H, 5.46; N, 3.62. Found: C, 74.33; H, 5.49; N, 3.54.

#### 4.1.13. *N*-{2-[2-(3,4-Dihydroxyphenyl)ethyl]phenyl}phthal imide: PPT-65

Mp 63.0–65.0 °C. $^1$H NMR (500 MHz, $CDCl_3$) $\delta$: 7.95 (dd, 2H, $J$ = 5.5, 2.4 Hz), 7.81 (dd, 2H, $J$ = 5.5, 2.4 Hz), 7.41–7.38 (m, 1H), 7.36–7.31 (m, 2H), 7.18 (dd, 1H, $J$ = 7.9, 1.2 Hz), 6.66 (d, 1H, $J$ = 7.9 Hz), 6.52 (d, 1H, $J$ = 1.8 Hz), 6.49 (dd, 1H, $J$ = 7.9, 1.8 Hz), 5.16 (s, 1H), 5.00 (s, 1H), 2.76 (m, 4H). FAB-MS $m/z$: 359 $[M]^+$, 360 $[M+H]^+$. HRMS (FAB) calcd for $C_{22}H_{17}NO_4$ 359.1158; found: 359.1127 $(M)^+$.

#### 4.1.14. *N*-{3-[2-(3,4-Dihydroxyphenyl)ethyl]phenyl}phthal imide: PPT-66

Mp 171.5–172.0 °C. $^1$H NMR (500 MHz, $CDCl_3$) $\delta$: 7.96 (dd, 2H, $J$ = 5.5, 2.4 Hz), 7.81 (dd, 2H, $J$ = 5.5, 2.4 Hz), 7.42 (t, 1H, $J$ = 7.9 Hz), 7.23 (dd, 1H, $J$ = 7.9, 2.4 Hz), 7.22 (dd, 1H, $J$ = 7.9, 1.8 Hz), 7.13 (m, 1H), 6.78 (d, 1H, $J$ = 7.9 Hz), 6.63 (dd, 1H, $J$ = 7.9, 1.8 Hz), 6.56 (d, 1H, $J$ = 1.8 Hz), 5.66 (s, 1H), 5.16 (s, 1H), 2.94–2.90 (m, 2H), 2.86–2.83 (m, 2H). FAB-MS $m/z$: 359 $[M]^+$, 360 $[M+H]^+$. Anal. Calcd for $C_{22}H_{17}NO_4$: C, 73.53; H, 4.77; N, 3.90. Found: C, 73.24; H, 4.84; N, 3.83.

#### 4.1.15. 4,5,6,7-Tetrachloro-*N*-{2-[2-(3,4-dihydroxyphenyl) ethyl]phenyl}phthalimide: PPT-67

Mp 227.0–229.5 °C. $^1$H NMR (500 MHz, $CDCl_3$) $\delta$: 7.41 (m, 1H), 7.36–7.32 (m, 2H), 7.14–7.13 (m, 1H), 6.66 (d, 1H, $J$ = 7.9 Hz), 6.53 (d, 1H, $J$ = 2.4 Hz), 6.49 (dd, 1H, $J$ = 7.9, 1.8 Hz), 5.09 (s, 1H), 4.94 (s, 1H), 2.76 (s, 4H). FAB-MS $m/z$: 495 $[M]^+$, 496 $[M+H]^+$, 497 $[M+2]^+$, 498 $[M+3]^+$, 499 $[M+4]^+$, 500 $[M+5]^+$. Anal. Calcd for $C_{22}H_{13}Cl_4NO_4$: C, 53.15; H, 2.64; N, 2.82. Found: C, 53.03; H, 2.88; N, 2.62.

#### 4.1.16. 4,5,6,7-Tetrachloro-*N*-{3-[2-(3,4-dihydroxyphenyl) ethyl]phenyl}phthalimide: PPT-68

Mp 208.0–210.0 °C. $^1$H NMR (500 MHz, $CDCl_3$) $\delta$: 7.43 (t, 1H, $J$ = 7.9 Hz), 7.24 (d, 1H, $J$ = 7.3 Hz), 7.20 (m, 1H), 7.10 (s, 1H), 6.78 (d, 1H, $J$ = 7.9 Hz), 6.63 (dd, 1H, $J$ = 7.9, 1.8 Hz), 6.58 (d, 1H, $J$ = 1.8 Hz), 5.53 (s, 1H), 5.15 (s, 1H), 2.93–2.91 (m, 2H), 2.85–2.82 (m, 2H). FAB-MS $m/z$: 495 $[M]^+$, 496 $[M+H]^+$, 497 $[M+2]^+$, 498 $[M+3]^+$, 499 $[M+4]^+$, 500 $[M+5]^+$. Anal. Calcd for $C_{22}H_{13}Cl_4NO_4 \cdot 2/3H_2O$: C, 51.90; H, 2.84; N, 2.75. Found: C, 51.70; H, 3.03; N, 2.60.

#### 4.1.17. 4,5,6,7-Tetrachloro-*N*-{3-[2-(4-methoxyphenyl) ethyl]phenyl}phthalimide: PPT-80

Mp 169.0–170.0 °C. $^1$H NMR (500 MHz, $CDCl_3$) $\delta$: 7.41 (t, 1H, $J$ = 8.5 Hz), 7.23–7.22 (m, 2H), 7.09 (d, 2H, $J$ = 8.5 Hz), 6.83 (d, 2H, $J$ = 8.5 Hz), 3.79 (s, 3H), 2.96–2.93 (m, 2H), 2.91–2.87 (m, 2H). FAB-MS $m/z$: 494 $[M+H]^+$, 495 $[M+2]^+$, 496 $[M+3]^+$, 497 $[M+4]^+$, 498 $[M+5]^+$. Anal. Calcd for $C_{23}H_{15}Cl_4NO_3 \cdot 1/4H_2O$: C, 55.28; H, 3.13; N, 2.80. Found: C, 55.28; H, 3.09; N, 2.78.

#### 4.1.18. 4,5,6,7-Tetrachloro-*N*-{3-[(1*E*)-2-phenylethenyl] phenyl}phthalimide: PPT-84

Mp 259.5–261.5 °C. $^1$H NMR (500 MHz, $CDCl_3$) $\delta$: 7.58–7.56 (m, 2H), 7.52–7.49 (m, 3H), 7.37 (t, 2H, $J$ = 7.9 Hz), 7.31–7.28 (m, 2H), 7.15 (d, 1H, $J$ = 16.8 Hz), 7.12 (d, 1H, $J$ = 16.8 Hz). FAB-MS $m/z$: 461 $[M]^+$, 462 $[M+H]^+$, 463 $[M+2]^+$, 464 $[M+3]^+$, 465 $[M+4]^+$, 466 $[M+5]^+$. Anal. Calcd for $C_{22}H_{11}Cl_4NO_2 \cdot 1/3H_2O$: C, 56.32; H, 2.51; N, 2.99. Found: C, 56.55; H, 2.56; N, 2.98.

#### 4.1.19. 4,5,6,7-Tetrachloro-*N*-{3-[2-(4-hydroxyphenyl) ethyl]phenyl}phthalimide: PPT-85

Mp 210.0–212.0 °C. $^1$H NMR (500 MHz, $CDCl_3$) $\delta$: 7.41 (t, 1H, $J$ = 7.3 Hz), 7.24–7.20 (m, 3H), 7.03 (d, 2H, $J$ = 8.5 Hz), 6.75 (d, 2H, $J$ = 8.5 Hz), 4.60 (br s, 1H), 2.95–2.92 (m, 2H), 2.89–2.86 (m, 2H). FAB-MS $m/z$: 479 $[M]^+$, 480 $[M+H]^+$, 481 $[M+2]^+$, 482 $[M+3]^+$, 483 $[M+4]^+$, 484 $[M+5]^+$. Anal. Calcd for $C_{22}H_{13}Cl_4NO_3$: C, 54.92; H, 2.72; N, 2.91. Found: C, 54.68; H, 2.82; N, 2.83.

#### 4.1.20. 4,5,6,7-Tetrachloro-*N*-{3-[(1*Z*)-2-phenylethenyl] phenyl}phthalimide: PPT-86

White powder from $CH_2Cl_2$/*n*-hexane. Mp 164.0–165.5 °C. $^1$H NMR (500 MHz, $CDCl_3$) $\delta$: 7.37–7.26 (m, 5H), 7.25–7.18 (m, 4H), 6.67 (d, 1H, $J$ = 12.2 Hz), 6.59 (d, 1H, $J$ = 12.2 Hz). FAB-MS $m/z$: 461 $[M]^+$, 462 $[M+H]^+$, 463 $[M+2]^+$, 464 $[M+3]^+$, 465 $[M+4]^+$, 466 $[M+5]^+$. Anal. Calcd for $C_{22}H_{11}Cl_4NO_2$: C, 57.05; H, 2.39; N, 3.02. Found: C, 56.81; H, 2.53; N, 2.93.

#### 4.1.21. 4,5,6,7-Tetrachloro-*N*-{4-[(1*Z*)-2-phenylethenyl] phenyl}phthalimide: PPT-87

White powder from $CH_2Cl_2$/*n*-hexane. Mp 155.5–157.5 °C. $^1$H NMR (500 MHz, $CDCl_3$) $\delta$: 7.58–7.49 (m, 1H), 7.38–7.18 (m, 8H), 6.67 (d, 1H, $J$ = 12.8 Hz), 6.59 (d, 1H, $J$ = 12.8 Hz). FAB-MS $m/z$: 461 $[M]^+$, 462 $[M+H]^+$, 463 $[M+2]^+$, 464 $[M+3]^+$, 465 $[M+4]^+$, 466 $[M+5]^+$. Anal. Calcd for $C_{22}H_{11}Cl_4NO_2 \cdot 1/3H_2O$: C, 56.32; H, 2.51; N, 2.99. Found: C, 56.35; H, 2.60; N, 2.96.

#### 4.1.22. 4,5,6,7-Tetrachloro-*N*-{3-[2-(3-methoxyphenyl) ethyl]phenyl}phthalimide: PPT-91

Mp 150.0–151.0 °C. $^1$H NMR (500 MHz, $CDCl_3$) $\delta$: 7.42 (t, 1H, $J$ = 7.9 Hz), 7.26–7.25 (m, 2H), 7.23 (m, 1H), 7.20 (t, 1H, $J$ = 7.9 Hz), 6.78 (d, 1H, $J$ = 7.3 Hz), 6.75 (dd, 1H, $J$ = 7.9, 1.8 Hz), 6.72–6.72 (m, 1H), 3.78 (s, 3H), 3.00–2.96 (m, 2H), 2.94–2.91 (m, 2H). FAB-MS $m/z$: 493 $[M]^+$, 494 $[M+H]^+$, 495 $[M+2]^+$, 496 $[M+3]^+$, 497 $[M+4]^+$, 498 $[M+5]^+$. Anal. Calcd for $C_{23}H_{15}Cl_4NO_3 \cdot 1/4H_2O$: C, 55.28; H, 3.13; N, 2.80. Found: C, 55.43; H, 3.11; N, 2.82.

#### 4.1.23. 4,5,6,7-Tetrachloro-*N*-{3-[2-(3-hydroxyphenyl) ethyl]phenyl}phthalimide: PPT-94

Mp 213.0–215.0 °C. $^1$H NMR (500 MHz, $CDCl_3$) $\delta$: 7.42 (t, 1H, $J$ = 7.9 Hz), 7.25–7.20 (m, 3H), 7.15 (t, 1H, $J$ = 7.9 Hz), 6.76 (d, 1H, $J$ = 7.9 Hz), 6.68 (dd, 1H, $J$ = 7.9, 2.4 Hz), 6.62 (t, 1H, $J$ = 1.8 Hz), 2.98–2.95 (m, 2H), 2.92–2.88 (m, 2H). FAB-MS $m/z$: 479 $[M]^+$, 480 $[M+H]^+$, 481 $[M+2]^+$, 482 $[M+3]^+$, 483 $[M+4]^+$, 484 $[M+5]^+$. Anal. Calcd for $C_{22}H_{13}Cl_4NO_3$: C, 54.92; H, 2.72; N, 2.91. Found: C, 54.68; H, 2.99; N, 2.77.

#### 4.1.24. 4,5,6,7-Tetrachloro-*N*-{3-[(1*E*)-2-(3,4-dimethoxyphenyl) ethenyl]phenyl}phthalimide: PPT-95

Mp 248.0–249.0 °C. $^1$H NMR (500 MHz, $CDCl_3$) $\delta$: 7.56–7.54 (m, 2H), 7.49 (t, 1H, $J$ = 7.9 Hz), 7.29–7.27 (m, 1H), 7.09 (d, 1H, $J$ = 16.2 Hz), 7.07–7.05 (m, 2H), 6.99 (d, 1H, $J$ = 16.2 Hz), 6.87 (d, 1H, $J$ = 7.9 Hz), 3.95 (s, 3H), 3.91 (s, 3H). FAB-MS $m/z$: 521 $[M]^+$, 522 $[M+H]^+$, 523 $[M+2]^+$, 524 $[M+3]^+$, 525 $[M+4]^+$, 526 $[M+5]^+$. Anal. Calcd for $C_{24}H_{15}Cl_4NO_4 \cdot 1/2H_2O$: C, 54.16; H, 3.03; N, 2.63. Found: C, 53.98; H, 3.03; N, 2.49.

Please cite this article in press as: Iwai, Y.; et al. *Bioorg. Med. Chem.* (2010), doi:10.1016/j.bmc.2010.05.035